Ocean Basin Geometry and the Salinification of the Atlantic Ocean

JOHAN NILSSON

Department of Meteorology, Bert Bolin Centre for Climate Research, Stockholm University, Stockholm, Sweden

PETER L. LANGEN

Danish Climate Centre, Danish Meteorological Institute, Copenhagen, Denmark

DAVID FERREIRA AND JOHN MARSHALL

Department of Earth, Atmospheric and Planetary Science, Massachusetts Institute of Technology, Cambridge, Massachusetts

(Manuscript received 20 June 2012, in final form 6 February 2013)

ABSTRACT

A coupled atmosphere–sea ice–ocean model is used in an aqua-planet setting to examine the role of the basin geometry for the climate and ocean circulation. The basin geometry has a present-day-like topology with two idealized northern basins and a circumpolar ocean in the south. A suite of experiments is described in which the southward extents of the two (gridpoint wide) ''continents'' and the basin widths have been varied. When the two basins have identical shapes, the coupled model can attain a symmetric climate state with northern deep-water formation in both basins as well as asymmetric states, where the deep-water formation occurs only in one of the basins and Atlantic–Pacific-like hydrographic differences develop. A difference in the southward extents of the land barriers can enhance as well as reduce the zonal asymmetries of the atmosphere–ocean circulation. This arises from an interplay between the basin boundaries and the wind-driven Sverdrup circulation, which controls the interbasin exchange of heat and salt. Remarkably, when the short ''African'' continent is located near or equatorward of the zero wind line in the Southern Hemisphere, the deep-water formation becomes uniquely localized to the ''Atlantic''-like basin with the long western boundary. In this case, the salinification is accomplished primarily by a westward wind-routed interbasin salt transport. Furthermore, experiments using geometries with asymmetries in both continental extents and basin widths suggest that in the World Ocean these two fundamental basin asymmetries should independently be strong enough for uniquely localizing the Northern Hemisphere deep-water formation to the Atlantic Ocean.

1. Introduction

In the present climate, the hydrography and the circulation in the North Atlantic and North Pacific are strongly asymmetric (e.g., Reid 1961; Weaver et al. 1999). The North Atlantic has higher sea surface salinities, and during winter deep convection occurs regionally. In the North Pacific, on the other hand, the sea surface salinities are lower, and a strong halocline prevents deep convection. As emphasized by Warren (1983), it is the basin difference in the salinity distributions, rather than in the temperature distributions, that makes the North Atlantic conducive for deep convection. The hydrographic asymmetry is closely linked to the global interocean circulation, which in the Atlantic Ocean is manifested by pronounced meridional overturning circulation and northward heat transport (e.g., Gordon 1986; Trenberth and Caron 2001). The question of what sets the asymmetry in hydrography and circulation between the North Atlantic and North Pacific remains controversial and numerous explanations have been proposed (e.g., Weaver et al. 1999; Huisman 2010).

At a fundamental level, however, two different explanations for the climatic differences between two basins can be distinguished. To begin with, the atmosphere–ocean circulation may have multiple equilibrium states: a present-day-like state with sinking and higher salinities in the North Atlantic and another state with sinking and higher salinities in the North Pacific (Walin 1985;

Corresponding author address: Johan Nilsson, Department of Meteorology, Stockholm University, SE-10691 Stockholm, Sweden. E-mail: nilsson@misu.su.se

DOI: 10.1175/JCLI-D-12-00358.1

Broecker et al. 1985). The underlying key mechanism is the salt–advection feedback described by Stommel (1961). This feedback can yield a spontaneous salinification; a faster flow yields higher salinities, which theoretically could localize the sinking to one of the two basins. In idealized geometries with two identical basins, ocean-circulation models have shown that the oceanic salt–advection feedback indeed can give rise to an ''Atlantic–Pacific''-like state (Marotzke and Willebrand 1991; Huisman et al. 2009). Increased net evaporation over the warmer and more saline basin forming the deep water is one atmosphere–ocean feedback that may further reinforce the salinity difference between the basins (Warren 1983; Broecker et al. 1985). However, an equilibrium state with deep-water formation in the Pacific appears to be difficult to obtain in ocean models with more realistic geometry and forcing, particularly when coupled to an atmosphere. In equilibrium states without deep-water formation in the North Atlantic, deep-water formation tends to relocate to the Southern Ocean rather than to the North Pacific (e.g., Manabe and Stouffer 1999; Dijkstra and Weijer 2005; Huisman 2010).

The other possibility is that the asymmetries in the geographical setting remove multiple equilibriums and uniquely locate the Northern Hemisphere deep-water formation to the Atlantic. If the geographically imposed basin differences in net precipitation and ocean circulation are pronounced enough, the salt–advection feedback will not be able to sustain an equilibrium with sinking and high salinities in the North Pacific. Geographical asymmetries proposed to promote a salinification of the Atlantic basin include

(i) the distribution of the mountain ranges, which via their effect on the atmospheric circulation can serve to make the Atlantic more saline; for example, the low-leveled Central America promoting freshwater export from the Atlantic (Weyl 1968; Schmittner et al. 2011; Sinha et al. 2012) and the Rockies affecting the surface winds and air temperature over the North Atlantic (e.g., Warren 1983; Seager et al. 2002; Czaja 2009);
(ii) the larger width of the Pacific, which reorganizes the atmospheric storm tracks and promotes a net water vapor export from the Atlantic (Ferreira et al. 2010) and can result in longer residence times of the water in the Pacific (De Boer et al. 2008);
(iii) the difference in southward extents of the American and African continents (e.g., Reid 1961; Gordon 1986; de Ruijter et al. 1999), which influence the pathways of the interbasin water exchange; and
(iv) regional details of the basin geometry such as the Mediterranean Sea and the Atlantic–Arctic connection (e.g., Reid 1979; Hughes and Weaver 1994; De Boer et al. 2008).

Clearly, there are several geographical asymmetries that seem to favor a salinification of the Atlantic basin. Still, it remains an essentially open question which of these geographical features must be present in order to uniquely localize the Northern Hemisphere deep-water formation to the Atlantic.

In the present study, we consider fundamental aspects of how the geometrical constraints of the ocean basins affect the climate and ocean circulation, building on results of Enderton and Marshall (2009) and Ferreira et al. (2010). Particularly, we seek to identify which coarse-grained features of the ocean basin geometry that can exert a control on the localization of deep sinking. To isolate the role of the ocean basin geometry, we disregard the details of the land–ocean distribution and focus on an aqua-planet setting in which narrow land barriers define the basins. The land barriers are flat and there are hence no orographic effects on the atmosphere. It should be noted that the tectonic evolution has created a range of ocean basin configurations with different topological features (see, e.g., Mikolajewicz et al. 1993; Barron et al. 1993). The present study, however, focuses on a basin geometry with topological properties similar to the present-day World Ocean, consisting of two northern basins that extend to the pole and a circumpolar Southern Ocean (see Fig. 1). Thus, the basin geometry is characterized by only three parameters: the relative basin widths and the termination latitudes of the two land barriers. To focus the investigation, we have chosen to exclude the geographical asymmetry related to the difference in northward extents of the real Atlantic and Pacific. Whereas this asymmetry arguably favors Atlantic sinking (e.g., Hughes and Weaver 1994), we will demonstrate that it is not necessary for uniquely localizing the sinking to an ''Atlantic''-like basin; asymmetries in the basin widths and the continental lengths are sufficient.

Using an atmosphere–ocean–sea ice model, we examine the climate and ocean circulation characteristics in a sequence of experiments in which the asymmetry of the basin geometry is gradually increased. We embark with an investigation of the climate states that can arise when the two basins have identical shapes, a problem that previously has been studied with ocean-only models (e.g., Marotzke and Willebrand 1991; Huisman et al. 2009). We then proceed to examine how a difference in the southward extent of the two land barriers influences the localization of the deep sinking. It is well established

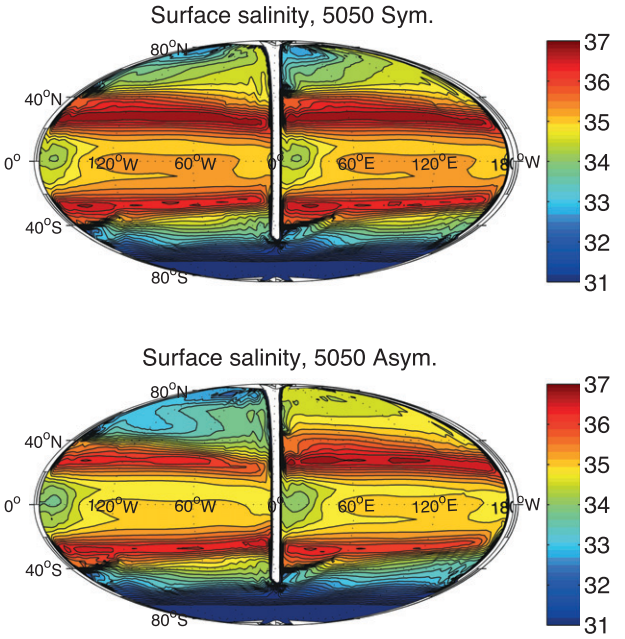

FIG. 1. Time-mean sea surface salinity for the 5050 geometry with equally wide basins and both continents terminating at 50°S. Note that a Mollwide projection is used which covers the entire sphere (the second land barrier is hardly visible but located near 180° on either side of the projection). (top) The symmetric equilibrium, for which time-mean circulation in and above the two basins are virtually identical. (bottom) One of the two asymmetric equilibriums with saline Atlantic-like conditions in the right-hand basin and fresher Pacific-like conditions in the left-hand basin. In this symmetric geometry, the initial conditions control which equilibrium the coupled atmosphere–ocean–sea ice model attains.

that the different southward extents of South America and Africa are important for the interocean water exchange, particularly for the transport of thermocline water from the Indo-Pacific to the Atlantic via the Agulhas Current system (Reid 1961; Gordon 1986; de Ruijter et al. 1999; Beal et al. 2011). One fundamental question we address is whether a difference in the continental lengths always serves to localize the deep-water formation to the Atlantic-like basin with the long western boundary, or if this basin-geometry asymmetry also can favor sinking in the ''Pacific like'' basin with the short western boundary.

Next, we recapitulate some key results of Ferreira et al. (2010) on the climate and ocean circulation in the configuration with one narrow and one wide basin, comparing these results with the present equal-width basin experiments. Finally, we consider the combined effect of asymmetries in basin widths and continental extents, examining the impact on the climate of an interchange of the locations of the short ''African'' and long ''American'' continent.

The remainder of the paper is organized as follows. Section 2 describes the model and the basin geometries. Section 3 examines the equilibrium climates obtained when the two basins have identical shapes. Section 4 examines how basin-geometry asymmetries affect the climate and ocean circulation, in particular their role for localizing the deep sinking. A discussion and conclusions are presented in section 5. In an appendix, transient experiments are described that provide additional insight on the processes that control the localization of the deep sinking.

2. Model description and general climate characteristics

a. Model description

We use the Massachusetts Institute of Technology (MIT) GCM in a coupled ocean–atmosphere–sea ice setup (Marshall et al. 1997b,a). As described in Adcroft et al. (2004), the model components use the same cubed sphere grid at a low-resolution C24 (24 × 24 points per face, yielding a resolution of 3.8° at the equator). The cubed sphere grid avoids problems associated with the converging meridians at the poles and greatly simplifies the implementation of a conservative interface between the two GCMs (Campin et al. 2008). As described in Marshall et al. (2004), isomorphisms between the equations of the large-scale flow in the atmosphere and the ocean were used to render atmosphere and ocean models from one hydrodynamical core. The atmospheric physics is of intermediate complexity, based on the simplified parameterizations primitive equation dynamics (SPEEDY) scheme (Molteni 2003) at low vertical resolution (five levels). Briefly, this method comprises a 4-band radiation scheme, a parameterization of moist convection, diagnostic clouds, and a boundary layer scheme. The 3-km-deep, flat-bottomed ocean model has 15 vertical levels, increasing from 30 m at the surface to 400 m at depth. Effects of mesoscale eddies are parameterized as an advective process (Gent and McWilliams 1990) and an isopycnal diffusion (Redi 1982), both with a transfer coefficient of 1200 $m^2\ s^{-1}$. Convective adjustment, implemented as an enhanced vertical mixing of temperature and salinity, is used to represent ocean convection (see Klinger et al. 1996). The background vertical diffusion is uniform and set to $3 \times 10^{-5}\ m^2\ s^{-1}$. The sea ice model is based on the Winton (2000) two-and-a-half-layer thermodynamic model. The prognostic variables are ice fraction, snow and ice thickness, and a two-level enthalpy representation that accounts for brine pockets and sea ice salinity, employing an energy-conserving formulation. There are

TABLE 1. Description and notation of the two-basin geometries for which simulations are performed. The ''Termination lat'' gives the southward extent of the two land barriers (narrow/wide) and ''Widths'' specify the zonal basin extents. In the N35W25 configuration, the narrow basin has the long western boundary; the opposite applies for the N25W35 configuration. The types of equilibriums are also indicated. For the unique equilibriums, the deep-water formation occurs in the narrow basin (the geometries with different basin widths) or the basin with the long western boundary (the geometries with equally wide basins). For the equilibriums labeled ''Asymm,'' the sinking can occur in either of the two basins.

Expt	Termination lat	Widths	Equilibriums
5050	50°S/50°S	180° each	Symm/Asymm
5035	50°S/35°S	180° each	Asymm
5010	50°S/10°S	180° each	Unique
3535	35°S/35°S	180° each	Asymm
3525	35°S/25°S	180° each	Unique
3510	35°S/10°S	180° each	Unique
N35W35	35°S/35°S	90° and 270°	Unique
N35W25	35°S/25°S	90° and 270°	Unique
N25W35	25°S/35°S	90° and 270°	Unique

no sea ice dynamics. The land model is a simple two-layer model with prognostic temperature, liquid groundwater, and snow depth. There is no continental ice. The land albedo is set to 0.25 plus a contribution from snow, if present. The snow albedo parameterization (identical over land and sea ice) depends on the snow depth, surface temperature, and snow age. Orbital forcing and CO_2 levels are assigned present-day values. The seasonal cycle is represented but there is no diurnal cycle.

b. Basin geometry

We consider a suite of aqua-planet basin configurations, topologically equivalent to the Double Drake geometry used by Ferreira et al. (2010), which have two northern basins and a circumpolar ocean in the south (see Table 1). In one configuration, the basins have the same zonal width (i.e., they are each 180° wide). In two of these experiments, the land barriers terminate at the same latitude, at 50° and 35°S, respectively. These geometries are referred to as 5050 and 3535. We have also examined geometries where the southward extents of the continents are different. These are referred to by the termination latitude of the long/short continent (i.e., 5035, 5010, 3525, and 3510). Further, we have examined three narrow–wide basin geometries where the two basins are 90° and 270° wide, respectively: one configuration where both continents terminate at 35°S (denoted N35W35), one in which the western boundary of the narrow/wide basin terminates at 35°S/25°S (denoted N35W25), and finally one where the extent of the land barriers are interchanged (denoted N25W35).

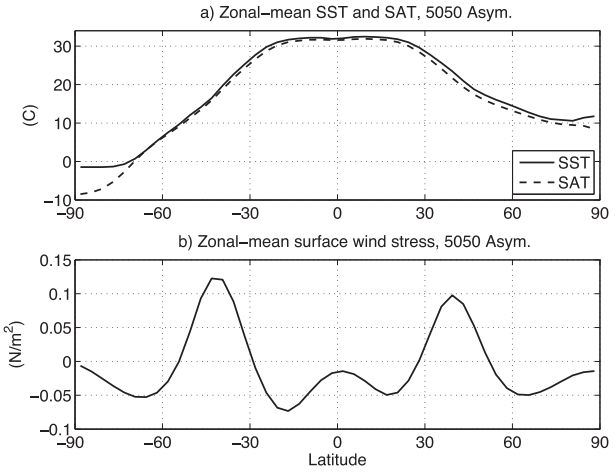

FIG. 2. (a) Zonal-mean SST and SAT and (b) the zonal component of the surface wind stress for the asymmetric 5050 equilibrium. In the Southern Hemisphere, the annual-mean sea ice edge is found near 78°S.

3. Spontaneous salinification in a fully symmetric geometry

In the 5050 and 3535 experiments, the two ocean basins have identical shapes. In these configurations, equilibrium climates may exist for which the oceanic as well as the atmospheric time-mean fields are nearly invariant for a zonal translation of 180° longitude. As illustrated in Fig. 1, we have indeed found such a symmetric equilibrium in the 5050 geometry. We have also obtained asymmetric states for which the deep-water formation occurs only in one of the basins. In the 3535 geometry, we have not found a symmetric equilibrium (see section 3d). The asymmetric 3535 equilibrium, however, is closely similar to the asymmetric state obtained in the 5050 geometry.

We will now go on to describe the climate and general circulation in the 5050 and 3535 experiments. We will also discuss the oceanic and atmospheric processes creating the salinification of the basin that forms the deep water in the identical-basin geometry. Note that in what follows, we present long-term time-mean diagnostics taken from the last few hundreds of years of solutions that are well equilibrated.

a. Zonal-mean climates and key zonal asymmetries

The zonal-mean structure of the atmosphere is highly similar between all the experiments with different basin geometry. Here, we briefly describe the zonal-mean climate features that are representative for all experiments and emphasize some of the key zonal asymmetries.

Figure 2 shows the zonal-mean sea surface temperature (SST), surface air temperature (SAT), and surface

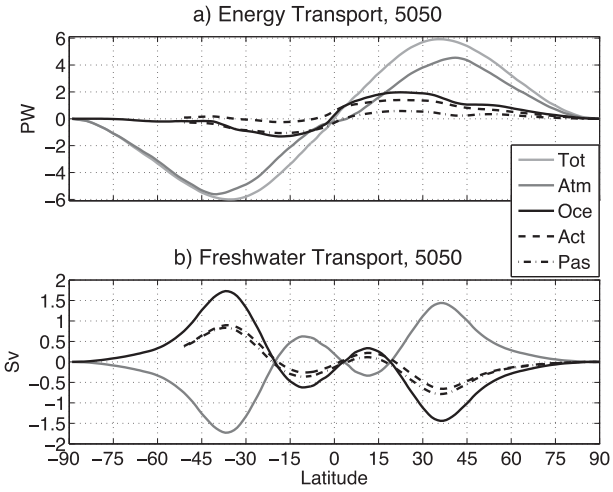

FIG. 3. (a) Meridional energy transports and (b) freshwater transports for the asymmetric 5050 equilibrium. The light gray lines show the total transports, whereas the dark gray and black lines give the atmospheric and oceanic transports, respectively. The dashed and dashed–dotted lines give the transports in the active basin (forming the deep water) and passive basin, respectively. The freshwater transport is measured in Sv (corresponding to a mass transport of about 10^9 kg s^{-1} condensed water.) Note that the net evaporation is slightly higher over the warmer basin forming the deep water, which consequently carries a smaller amount of freshwater southward than the colder basin.

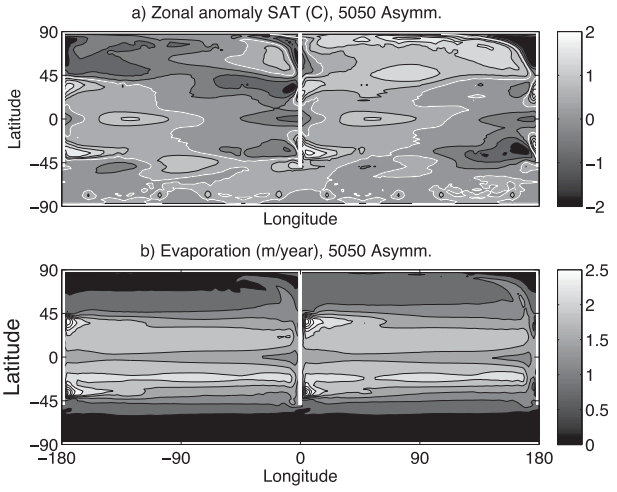

FIG. 4. The zonal anomaly in (a) SAT (contour interval of 0.5°C; thick white line is the 0°C contour) and (b) the surface evaporation (contour interval of 0.4 m yr^{-1}) for the asymmetric 5050 equilibrium. The active basin, forming the deep water, is located to the right.

wind stress for the asymmetric 5050 equilibrium. The annual-mean SST in the high northern latitudes is about 10°C, whereas it is at the freezing point of seawater in the high southern latitudes. The global mean surface air temperature, which is near 22°C in all experiments, is higher than on the earth. This is a feature of many coupled aqua-planet models, where a low surface albedo and a high heat capacity of the essentially ocean-covered planets contribute to give a warm climate (Smith et al. 2006; Enderton and Marshall 2009; Ferreira et al. 2010). The surface winds are qualitatively Earthlike, with slightly stronger winds in the Southern Hemisphere where the equator-to-pole temperature difference is larger than in the Northern Hemisphere. The meridional transports of heat and freshwater are shown in Fig. 3. As discussed by Enderton and Marshall (2009) and Ferreira et al. (2010), the present aqua-planet model yields meridional energy transports in the atmosphere and the ocean that are in broad agreement with observational estimates (see Fig. 1 in Ferreira et al. 2010). The total energy and freshwater transports and their partitioning between the ocean and the atmosphere are essentially the same for all the two-basin geometries considered in the present paper. Figure 3 shows that the atmosphere carries freshwater equatorward between roughly 20°S and 20°N, and poleward outside the deep tropics. In the model, the precipitation on the land points is routed zonally to the ocean and equally divided between the two basins. Thus, conservation of water implies that in a steady state, the oceanic and atmospheric meridional freshwater transports have the same magnitude but opposite directions.

Figure 4 shows the zonal anomaly in surface air temperature and the surface evaporation for the asymmetric 5050 equilibrium. In the present model, which has very narrow and flat continents, the zonal anomalies are created chiefly by the gyre-like ocean circulation within the basins. The main interbasin difference in SAT is a large-scale pattern of slightly elevated temperatures over the basin forming the deep water (see Fig. 4a). The highest surface evaporation is collocated with the poleward western boundary currents near the edge of the subtropics. The evaporation pattern with strong zonal variations seen in Fig. 4b is a common feature in all experiments. This proves to be important for the freshwater basin budget in geometries with different basins widths, an issue that we will return to.

b. Ocean circulation characteristics

Figures 5 and 6 illustrate the zonal-mean salinity and meridional overturning for the symmetric and the asymmetric 5050 equilibriums. The asymmetric 5050 equilibrium is qualitatively representative also for the asymmetric equilibriums obtained in the other basin configurations. Note that no deep-water formation occurs in the Southern Ocean in any of our aqua-planet simulations, where a strong halocline is encountered in the high latitudes. The absence of deep-water formation

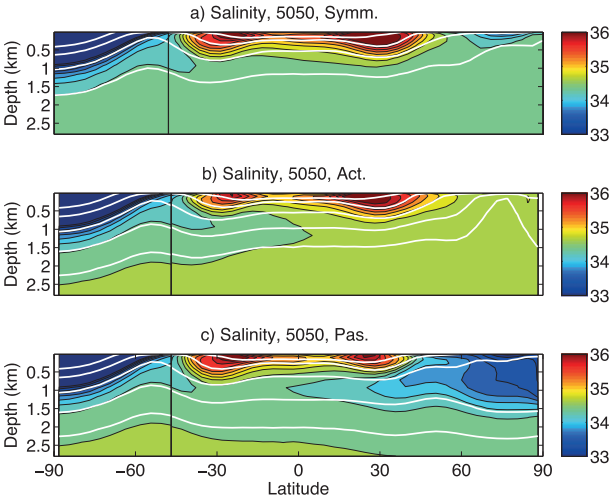

FIG. 5. Zonal-mean salinity for the (a) symmetric and (b),(c) asymmetric equilibriums in the 5050 experiments. The symmetric equilibrium shows the global zonal mean, whereas (b) and (c) show the zonal mean in the ''active'' and the ''passive'' basin, respectively. South of 50°S (denoted by vertical black line), in the circumpolar Southern Ocean, the global zonal-mean fields are illustrated. The white contours indicate the potential density surfaces 26.7, 26.5, 26.0, 25.0, and 24.0 kg m^{-3}.

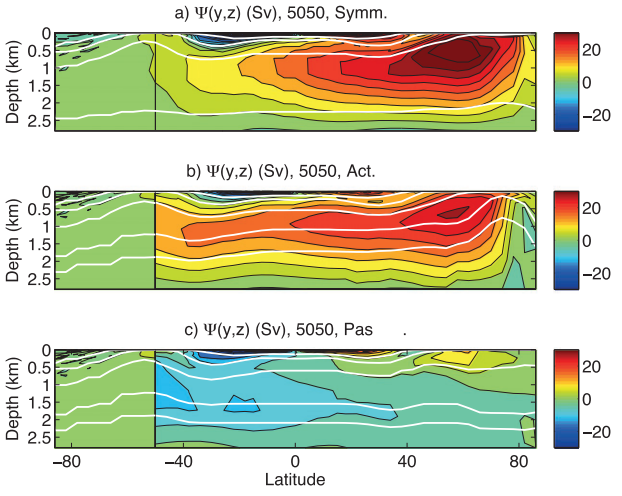

FIG. 6. Meridional overturning $\Psi(y, z)$ for the (a) symmetric and (b),(c) asymmetric equilibriums in the 5050 experiments. The contour interval is 4 Sv. Panel (a) shows the global overturning. Panel (b) and (c) show the overturning in the ''active'' and ''passive'' basin, respectively; south of 50°S, the global $\Psi(y, z)$ is shown. Positive Ψ values indicate a clockwise rotating cell. Note that $\Psi(y, z)$, which includes the Eulerian and the Gent and McWilliams (1990) bolus transports, has first been computed in potential density coordinates and then mapped into z-coordinates using a mean isopycnal depth $\hat{z}(y, \sigma)$. The white contours show $\hat{z}(y, \sigma)$ for the potential density surfaces 26.6, 26.5, 26.0, 25.0, and 24.0 kg m^{-3}.

may be related to the lack of continental shelves and topography in the Southern Ocean (e.g., Gill 1973; Toggweiler and Samuels 1995b).

For the symmetric equilibrium, the flow and hydrography in the mid-to-high northern latitudes share more features with the Atlantic than the Pacific Ocean. A striking feature of the asymmetric flows is the emergence of one Atlantic-like and one Pacific-like basin. The former basin, where the deep water is formed, is more saline and referred to as the *active basin*. In the other basin, referred to as the *passive basin*, a strong halocline is encountered in the north. Clearly, the transition from the symmetric to the asymmetric flow in the identical-basin geometry entails a dramatic reorganization of the salinity field, between the two basins as well as vertically.

In the symmetric equilibrium, the upwelling that balances the northern sinking occurs mainly near and north of the equator. In the asymmetric equilibrium, the overturning is markedly different in the two basins. In the active Atlantic-like basin, there is a ''swift'' main overturning cell, associated with an import and northward flow of water of low-to-intermediate densities that feeds the northern sinking. In the passive basin, on the other hand, the overturning is weak and shallow in the high northern latitudes. In the deep passive basin, the overturning is reversed with an inflow of deep water and general upwelling. The overturning circulation is closely associated with the meridional oceanic heat transport, yielding a stronger northward heat transport in the active than in the passive basin (Fig. 3). As shown in Fig. 6, the meridional overturning is weak in the Southern Ocean, where also the ocean heat transport is small.

c. *Mechanisms for salinification and desalinification*

It is primarily atmospheric dynamics that shapes the surface freshwater flux [defined as evaporation minus precipitation ($E - P$)] pattern and hence the oceanic freshwater transport. Accordingly, fundamental coupled atmosphere–ocean constraints control the broad features of the sea surface salinity distribution (e.g., Stommel and Csanady 1980; Nilsson and Körnich 2008). However, internal ocean dynamics and atmosphere–ocean feedbacks have the capacity to modify the salinity contrast between the basins and the meridional salinity gradients within the basins. Figure 5 reveals that compared to the symmetric equilibriums, the active basin is more saline and the passive basin is less saline when the flow is asymmetric. There are three main mechanisms that can create the differences in the salinity fields: changes in the ocean circulation within the basins, changes in the $E - P$ field, and changes in the interocean exchange of salt. To discuss the first two mechanisms qualitatively, we write the steady-state salinity balance as (see appendix A for details of the salt and freshwater budgets

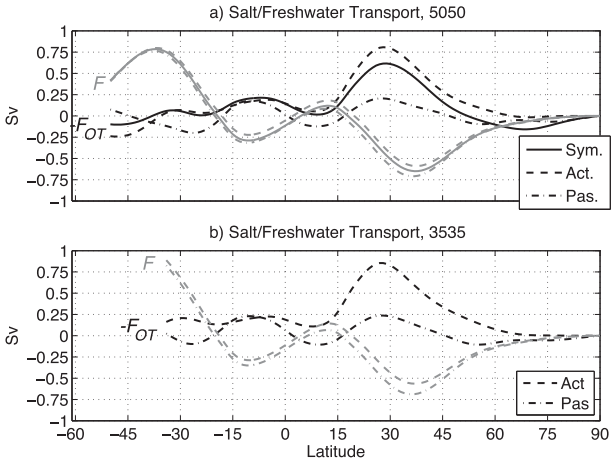

FIG. 7. Oceanic freshwater transports for the (a) 5050 and (b) 3535 experiments. Gray lines show the total transport F and the black lines show $-F_{\mathrm{OT}}$. Here, F_{OT} is the freshwater transport carried by the meridional overturning circulation; see Eq. (3). Dashed and dashed–dotted lines represent the active and passive basin transports, respectively. In (a) the solid lines represent the basin-mean transports of the symmetric 5050 equilibrium.

$$\Delta S\Psi + S_0 F = 0, \tag{1}$$

where Ψ is a meridional volume transport, ΔS a flow-weighted salinity difference, S_0 the mean salinity, and F the oceanic freshwater transport. Roughly, we expect that ΔS reflects the surface salinity difference between the Northern Hemisphere subtropics and high latitudes. For small changes one has $\delta\Delta S\Psi + \Delta S\delta\Psi + S_0\delta F = 0$, implying that

$$\frac{\delta\Delta S}{\Delta S} = -\frac{\delta\Psi}{\Psi} - \frac{\delta F}{F}, \tag{2}$$

where the quantities in the denominator represent a reference state. Equation (2) shows that if flow strength increases while F is preserved, the salinity contrast will diminish. This inverse relation between the flow speed and the salinity contrast is a key element in the classical model of Stommel (1961), which can have two steady-state solutions: a swift thermally dominated flow with a small salinity contrast and a slow salt-dominated flow with a large salinity contrast.

Figure 7a shows that compared to the symmetric equilibrium, the net freshwater input north of 30°N is reduced in the active and enhanced in the passive basin. Near 30°N, $|\delta F/F| \approx 10\%$, reflecting changes in the $E - P$ acting to reduce (enhance) the meridional salinity contrast in the northern active (passive) basin. Also, the flow changes contribute to the salinification. Compared to the symmetric equilibrium, the maximum meridional overturning is strengthened by about 50% in the active basin and reduced a comparable amount in the passive basin. It should be noted that the change in flow between symmetric and asymmetric equilibriums is primarily associated with the reorganization of the density distribution. There are also differences in surface winds between the two equilibriums. However, the related differences in wind-driven circulation are small enough that they can be neglected in this discussion.

To estimate the salinification because of changes in $E - P$ and circulation, we introduce a measure of the freshwater transport carried by the overturning circulation (cf. Rahmstorf 1996),

$$F_{\mathrm{OT}}(y) = -\frac{1}{S_0}\int\int_{A_{\mathrm{xz}}} (\overline{S} - S_0)\overline{v}\, dA, \tag{3}$$

where the overbar denotes the zonal mean, A_{xz} a zonal–vertical cross section, S the salinity, and v the meridional velocity. The remainder of the oceanic freshwater transport is carried by the azonal component F_{AZ} (i.e., $F = F_{\mathrm{OT}} + F_{\mathrm{AZ}}$). Figure 7 shows the net freshwater transport F and $-F_{\mathrm{OT}}$, which is proportional to the salt transport resulting from the overturning. In the Northern Hemisphere, the overturning circulation generally carries salt northward (i.e., $-F_{\mathrm{OT}} > 0$). South of 15°S, the azonal flow tends to dominate the salt transport. Clearly, the northward salt transport resulting from the overturning is magnified in the active basin. Near 30°N it is about 30% stronger than in the symmetric equilibrium. Thus, the change in F_{OT} is larger than the $E - P$ related change in the net oceanic freshwater transport F.

This qualitative analysis suggests that the changes in flow strength are the main cause of the salinity difference between the symmetric and asymmetric states in the 5050 experiments; the salinification of the active basin is primarily created by the oceanic salt–advection feedback. However, the stronger net evaporation that develops over the active basin is a positive feedback, reinforcing the basin differences in flow and hydrography (e.g., Warren 1983; Broecker et al. 1985). It should be underlined that this spontaneous salinification does not require the presence of any geographical asymmetries.

Next, consider the possible effects of interocean salt exchange for the salinification of the basin forming the deep water. Here, the prototype example is the Agulhas leakage of warm saline thermocline waters from the Indo-Pacific to the Atlantic (Gordon 1986; Rahmstorf 1996; Beal et al. 2011). The key idea is that the Atlantic meridional overturning circulation carries saline Agulhas leakage water northward through the Atlantic and returns less saline deep water southward. If the associated salt import exceeds the amount required by the

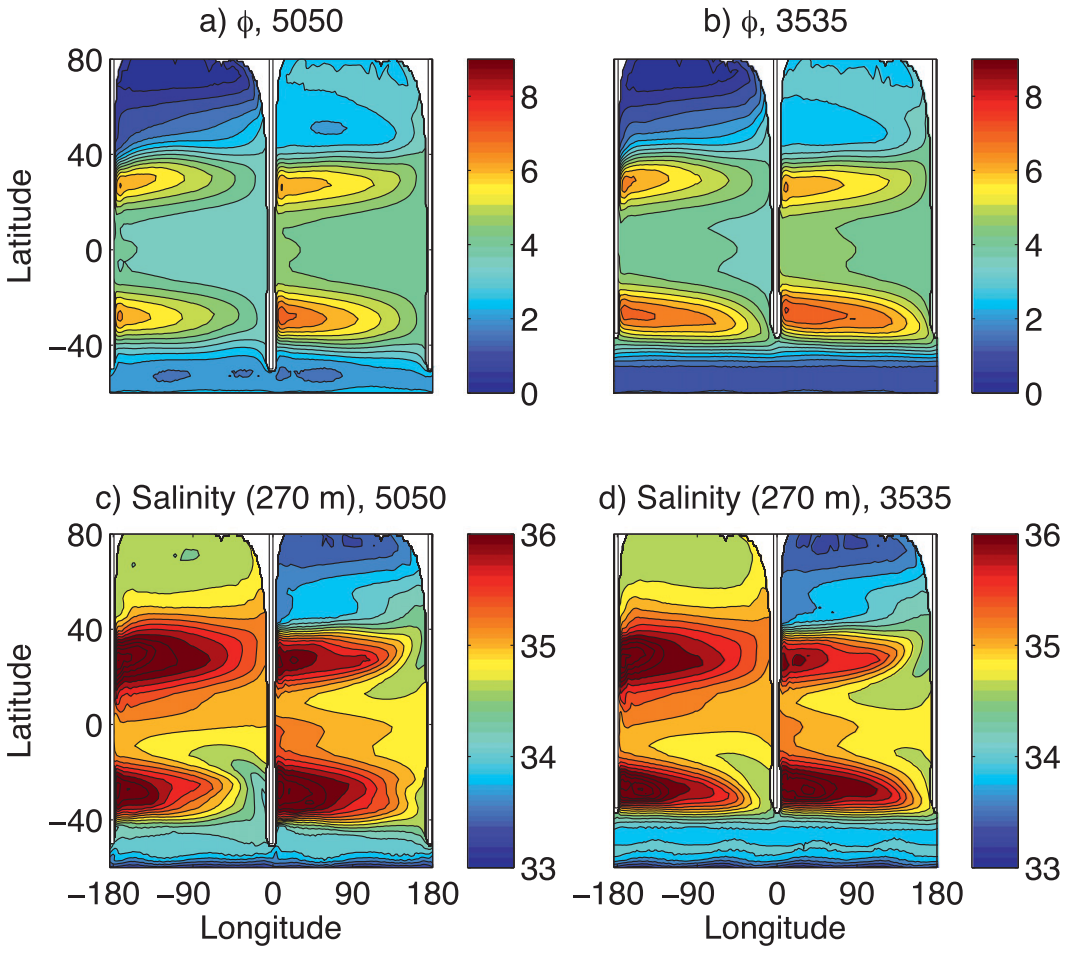

FIG. 8. Potential energy anomaly ϕ and salinity at 270 m for (a),(c) the asymmetric 5050 and (b),(d) the 3535 experiments. The ϕ field, illustrating the circulation of thermocline water, is computed relative to 1000 m and given in units of 10^3 m^3 s^{-1}; the contour interval is 0.5×10^3 m^3 s^{-1}. Note that $f^{-1}\mathbf{k} \times \nabla\phi$ represents the depth integrated thermal wind flow from z_{ref} to the surface assuming a level of no motion at z_{ref}, where f is the Coriolis parameter [see Eq. (4)]. In the subtropical gyres the ϕ field corresponds to a flow on the order of 40 Sv in each basin.

basin freshwater budget, the Atlantic salinity will increase. A steady state can be attained when the South Atlantic is saline enough that the necessary southward salt export is accomplished by downgradient transport as a result of horizontal gyre and eddy circulation.

It should be underlined that the meridional overturning circulation in the real Atlantic is supplied by both Agulhas leakage water and less saline water from the Southern Ocean (Gordon 1986; Rintoul 1991). If the supply is sourced primarily from the Southern Ocean, the overturning would export salt from the Atlantic. However, observations and ocean reanalyses are not conclusive regarding the relative source contributions and the salt transport direction because of the overturning circulation at the entrance of the South Atlantic (Bryden et al. 2011; J. R. Toggweiler et al. 2013, personal communication; Hawkins et al. 2011). In what follows, we will show that the basin geometry plays a critical role for the partitioning between the saline and fresh source waters that feed the overturning circulation in the active basin.

In the 5050 geometry, the upper ocean is less saline than the deep ocean near the southern basin boundaries (Fig. 5). As a result, the overturning circulation exports salt from the basin forming the deep water (Fig. 7). In the 3535 geometry, where the upper ocean is more saline than the deep ocean near the southern basin boundaries, the overturning carries salt into the active basin. The differences in freshwater transport in the two basin geometries reflect the interocean exchange of thermocline water. This can be inferred from Fig. 8, showing the thermocline salinity and gyre circulation in two experiments. As a proxy for the depth-integrated thermocline flow, we use a potential energy anomaly defined by

$$\phi = -\int_{z_{\text{ref}}}^{0} zb\,dz\,. \tag{4}$$

Here, $b = g[\rho_0 - \sigma(S, \theta)]/\rho_0$ defines a buoyancy anomaly, where g is the acceleration of gravity, $\sigma(S, \theta)$ the potential density, and ρ_0 a constant reference density; z is the vertical coordinate and z_{ref} a reference level (taken to be -1000 m). Figure 8 does not reveal any pronounced ''Agulhas''-like interbasin exchange of thermocline waters. Rather, water with relatively low salinity tends to enter the basins near the eastern boundaries. In the 5050 experiment, the water entering the active basin seems to originate mainly from the subpolar gyres and the Southern Ocean; a flow resembling the ''cold water path'' from the Southern Ocean northeastward into the South Atlantic (Gordon 1986; Rintoul 1991). However, we will see that dissimilar continental lengths can strongly enhance the interbasin exchange of thermocline water.

d. Symmetric versus asymmetric equilibriums

We obtained the 5050 symmetric state by initializing the model with zonally symmetric fields, computed from an equilibrated N35W35 simulation. When we applied the same procedure in the 3535 geometry, the flow initially remained nearly identical in the two basins, gradually adjusting toward a symmetric state. After about 500 yr, asymmetric perturbations emerged and amplified, causing a transition to the asymmetric equilibrium. We also did a simulation using zonally symmetric initial conditions based on the fields of the previous experiment near year 500. Also this restart experiment began to drift toward the asymmetric state after a couple of hundred years.

Thus, our simulations indicate that the symmetric 3535 state is unstable or, at the least, less robust than that in the 5050 geometry. It is relevant to note that in the symmetric 5050 equilibrium, the overturning circulation exports salt from the northern basins (see Fig. 7). This can entail a stabilizing feedback on the symmetric equilibrium: if the overturning in one of the basins increases the salt export also increases. With some delay, the salinity and hence the density of the deep water formed in the north are likely to decrease. This is expected to reduce the overturning strength in the perturbed basin, thereby restoring the symmetric state. In the 3535 geometry, where the upper ocean is more saline than the deep ocean near the southern basin boundaries, the overturning in a symmetric state would presumably carry salt into the northern basin. The fact that $-F_{\text{OT}}$ for the symmetric 5050 state becomes slightly positive near 35°S supports this notion. Thus, in the 3535 geometry, there is presumably a positive feedback between perturbations in overturning and basin salinity which acts to destabilize the symmetric equilibrium.

It is important to recognize that the wind-forced equatorward Ekman transport in the circumpolar Southern Ocean drives an overturning component that is nearly adiabatic below the surface mixed layer (e.g., Toggweiler and Samuels 1995a; Wolfe and Cessi 2011; Marshall and Speer 2012). This overturning component serves to sustain the northern sinking both in the symmetric and asymmetric states. The Ekman transport in the circumpolar channel is 30 Sv (1 Sv $\equiv 10^6$ m^3 s^{-1}) near 35°S, but only 15 Sv near 50°S; it is 40 Sv near 40°S where the surface westerlies peak. Accordingly, the Ekman transport is stronger and convergent just south of the basin entrances in the 3535 geometry, whereas it is weaker and divergent in the 5050 geometry. The features of Ekman transport near the basin entrances may well influence the stability of the symmetric states. We do not pursue this issue further here, but we note that Johnson et al. (2007) have discussed some aspects of the interplay between salt–advection feedback and Ekman-forced meridional overturning in a single basin setting.

4. Asymmetric basin geometries

a. The effect of different southward extent of the land barriers

To begin with, we consider how a difference in the southward extent of the two basin boundaries affects the asymmetric climate states when the basins are equally wide. Given the strong zonal transports in the ocean thermocline associated with the wind-driven gyre circulation, which can be inferred from Fig. 8, we anticipate that the termination latitude of the continents relative to the zonal surface winds will be important. From the Sverdrup relation (Sverdrup 1947), one expects that the transition from westward to eastward flow in the subtropical gyre is encountered near the latitude where the curl of surface wind stress reaches its maximum. This latitude is found roughly where the surface winds in the subtropics shift from easterly to westerly. In the present simulations, the subtropical maximum of the zonal-mean curl τ is found near 30°S (see Fig. 2). We have therefore conducted experiments with the short continent terminating equatorward as well as poleward of the subtropical zero wind line near 30°S.

1) TERMINATING THE SHORT CONTINENT EQUATORWARD OF THE ZERO WIND LINE

In the 3525, 3510, and 5010 experiments, the short continent terminates equatorward of the zero wind line

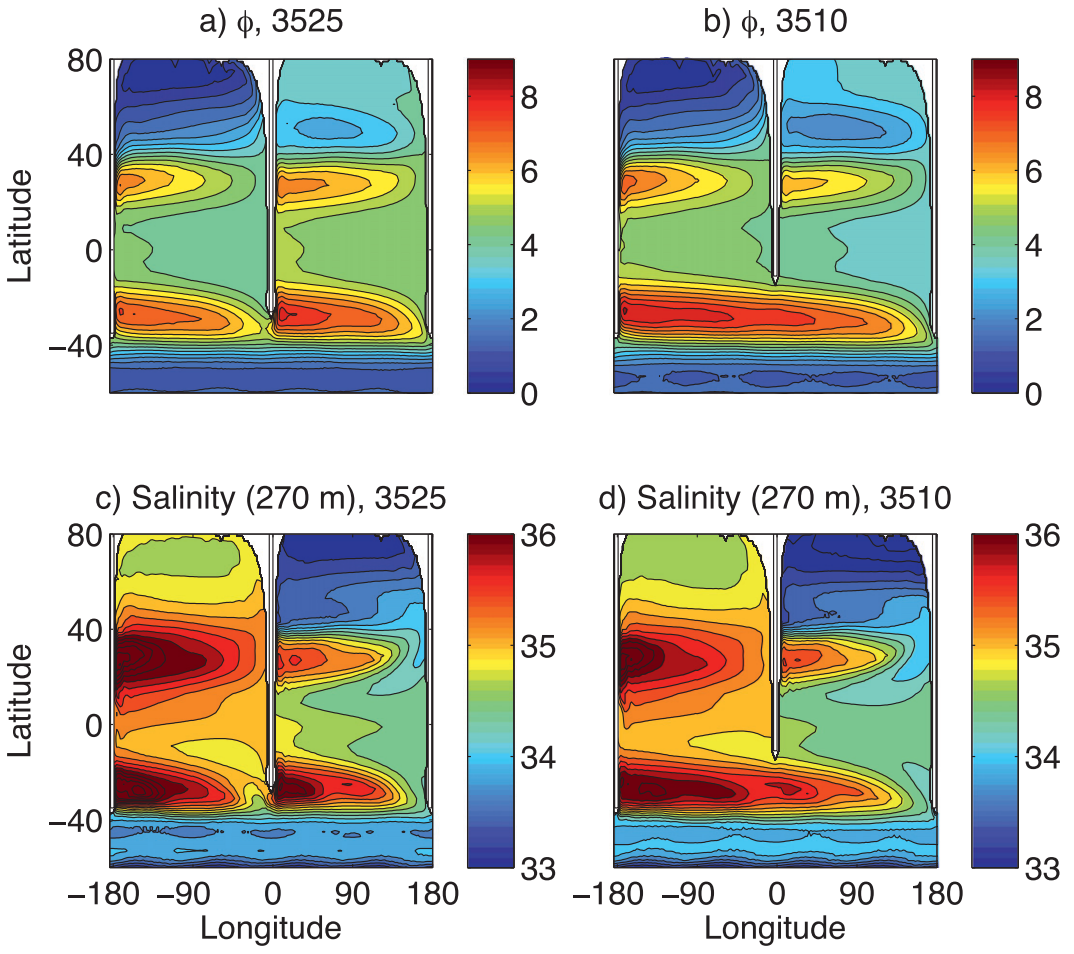

FIG. 9. As in Fig. 8, but for (a),(c) the 3525 and (b),(d) the 3510 experiments. Note in both geometries, the deep-water formation is uniquely localized to the basin with the long western boundary.

and, as anticipated, the flow of thermocline water is westward just south of the short continent (see Fig. 9). For these basin geometries, our numerical experiments suggest that there is only one equilibrium state: the deep water is formed in the basin with Atlantic-like geometry having the long continent as its western boundary. In appendix B, we examine how the model evolves to these unique equilibrium states from initial states with high salinity and sinking in the basin with Pacific-like geometry.

In the 3525, 3510, and 5010 experiments, the basin asymmetry in flow and hydrography becomes amplified relative to the case where the two continents extend equally far south. When the short continent is shifted equatorward, the increased basin asymmetry is manifested in the following features.

(i) The surface salinity decreases in the northern passive basin, where also the halocline becomes more pronounced. The changes in salinity are weaker in the active basin (Fig. 10).

(ii) The northward heat transport is increased (decreased) in the active (passive) basin (Fig. 11a).

(iii) The deep overturning cell slightly amplifies in the active basin, whereas the intermediate cell in the passive northern basin decreases (not shown).

(iv) The Northern Hemisphere basin difference in $E - P$ increases: north of 30°N the net freshwater input to the active (passive) basin decreases (increases). This coupled response serves to amplify the basin contrasts.

We note that the response of the hydrography and ocean circulation to an equatorward shift of the continent obtained here is similar to the response that Sijp and England (2008, 2009) obtained when they shifted the Southern Hemisphere wind field poleward in a model with realistic basin geometry.

Figure 9 illustrates the interbasin exchange of thermocline waters in the 3525 and 3510 experiments. In the 3525 experiment, the ϕ field indicates that a fraction of

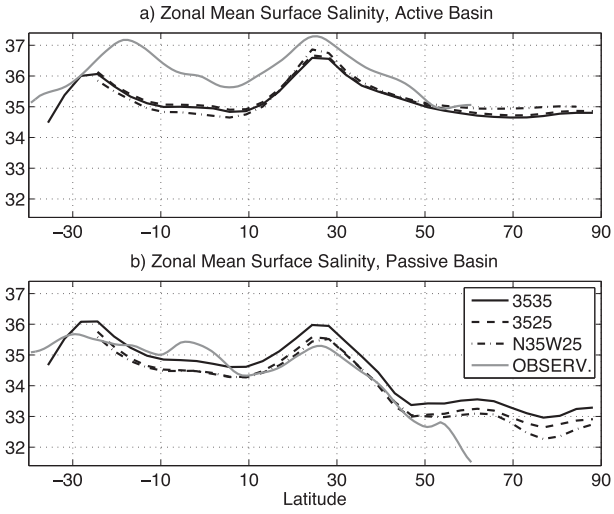

FIG. 10. Zonal-mean surface salinity for the 3535 (solid lines), 3525 (dashed lines), N35W25 (dashed–dotted lines) experiments. (a) Shows the salinity in the active basin and (b) shows the salinity in the passive basin. The gray lines show the surface salinity in the Atlantic at 30°W in (a) and the Pacific at 170°W in (b).

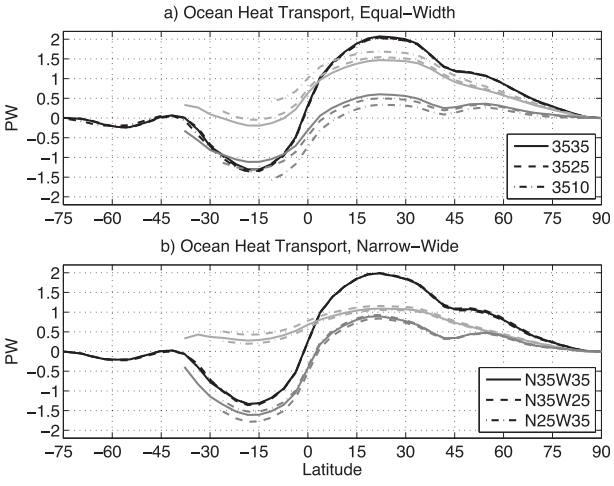

FIG. 11. Ocean heat transport for the 35-suite (a) equal basin width and (b) narrow–wide basin experiments. Black lines show the total heat transport and light (dark) gray lines show the heat transport in the active (passive) basin. In (a), the 3535 (solid lines), 3525 (dashed lines), and 3510 (dashed–dotted lines) experiments, which have two equally wide basins, are shown. In (b), the N35W35 (solid lines), N35W25 (dashed lines), and N25W35 (dashed–dotted lines) experiments, which have one 90°- and one 270°-wide basin, are shown; in these experiments the sinking occurs in the narrow basin.

the western boundary transport in the passive basin is deflected westward into the active basin near the tip of the short continent. The salinity field at 270 m shows a plume with high salinities that extends into the active basin west of the tip of the short continent. However, the bulk of the thermocline water in passive-basin subtropical gyre turns eastward near the tip of the short continent. In fact, the flow near the termination of the short continent shares some qualitative features with the flow in the Agulhas current system near the southern tip of Africa (e.g., de Ruijter et al. 1999; Beal et al. 2011). A fraction of the Agulhas Current, that flows southward along the coast of East Africa, retroflects eastward near Cape of Good Hope. Another fraction sheds off in eddies that drift northwestward into the Atlantic, a phenomena referred to as Agulhas leakage. In coarse-resolution models, as the present one, the leakage transport is produced by the time-mean flow and the parameterized eddy transports (e.g., de Ruijter et al. 1999; Corell et al. 2009). Regardless of the detailed dynamics, however, the interbasin exchange of thermocline water in the 3525 experiment mainly follows a westward ''warm water path'' as described by Gordon (1986).

The 3510 and 5010 experiments reveal a slightly different regime of interbasin exchange (see Figs. 9 and 12). Here, there is a single subtropical gyre in the Southern Hemisphere with its western boundary on the long continent. Thus, there is an efficient communication between the active basin and the common sector having the long continent as both western and eastern boundaries. As a result, the bulk of the water subducted in the subtropical gyre moves northwestward into the active basin, further strengthening the warm water path of the interocean exchange. Qualitatively, this flow pattern is expected from theoretical models of the ventilated thermocline (e.g., McCreary and Lu 1994; Pedlosky 1996).

Remarkably, Fig. 10 shows that the zonal-mean surface salinity in the active basin is only weakly affected by the geometrically induced changes in interbasin circulation. In the northern part of the active basin, where deep convection occurs, the surface salinity remains close to the mean deep-water salinity, which increases slightly when the continent is shifted equatorward. The response is more pronounced in the passive basin, where the surface salinity is decreased and the northern halocline becomes stronger.

The meridional ocean heat transport, shown in Fig. 11a, illustrates that the total heat transport is essentially insensitive to the changes of the continental extents. However, the heat transport from the passive to the active basin increases when the short continent is moved equatorward. Primarily, this reflects a strengthening of the warm water path flow of thermocline water from the passive to the active basin. A striking feature is the strong heat transport crossing the basin entrances in the 3510 experiment. In the 3535 experiment, the tropical oceanic heat uptake, which occurs between about 15°S and 20°N, is nearly identical in the two basins. When the short continent is poleward of the subtropical zero wind line, the tropical heat gain becomes stronger in the

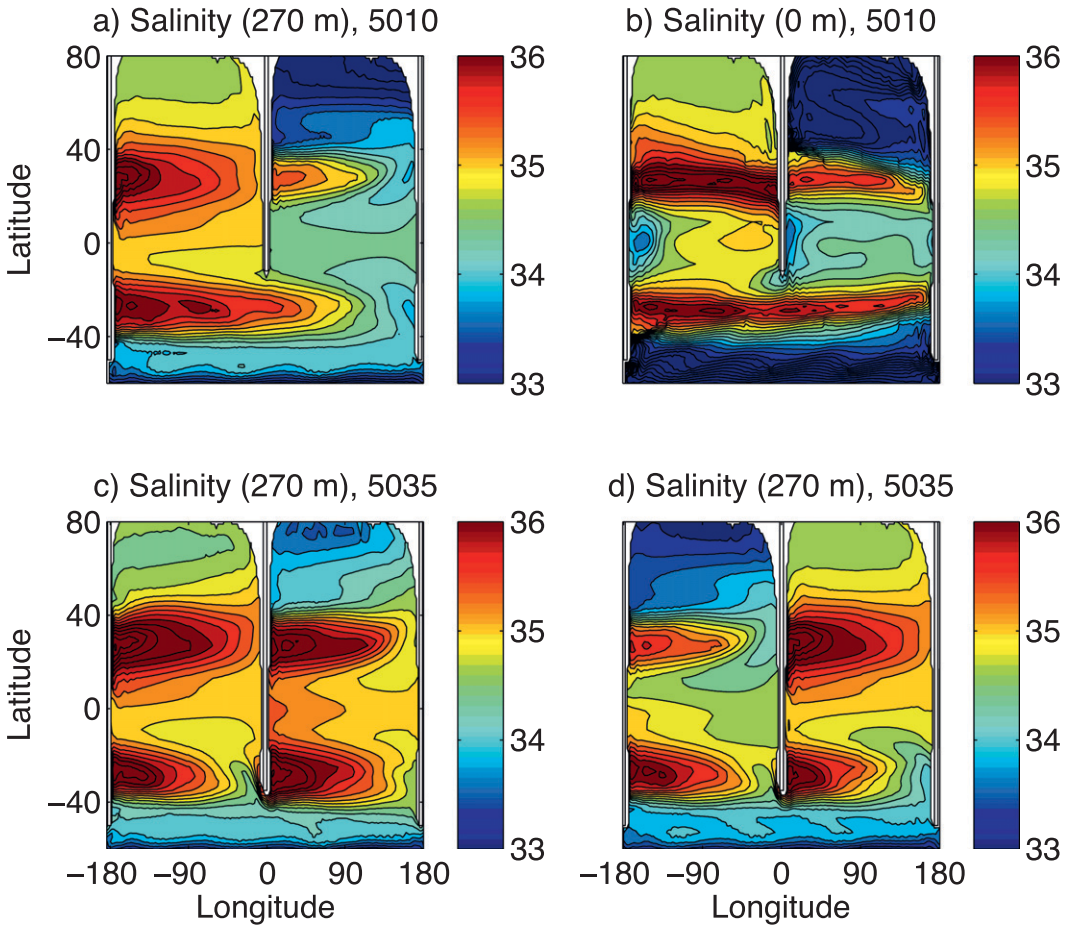

FIG. 12. Salinity fields from the (a),(b) 5010 and (c),(d) 5035 experiments. In the latter geometry, there are two equilibriums: one with sinking in the Atlantic basin shown in (c) and one with sinking in the Pacific basin shown in (d). The salinity at 270 m is shown, except for (b), which shows the surface salinity.

passive basin whereas it becomes weaker in the active basin (see also Fig. 15).

The active basin meridional overturning circulation and its associated salt transport [i.e., $-S_0F_{OT}$; see Eq. (3)] in the 3525, 3510, and 5010 experiments (not shown) are only marginally stronger than in the 3535 experiment. Thus, the enhancement of the northward heat transport in the active basin, associated with a shortening of the continent, is primarily the result of a temperature increase of the waters that enter the active basin. The weak response of the salt transport associated with the overturning partly reflects that when the continent is shortened, the salinity increases both in the upper-ocean water entering and the deep-ocean water exiting the active basin.

2) TERMINATING THE SHORT CONTINENT POLEWARD OF THE ZERO WIND LINE

In the 5035 geometry, the short as well as the long continents end in the latitude band of westerly surface winds. Here, the flow of thermocline water in the subtropical gyre is essentially eastward poleward of the short continent (see Fig. 13). In this geometry, we have obtained two equilibriums: depending on the initial conditions, the deep-water formation can occur in the basin with the long or the short western boundary.

When the deep-water formation occurs in the Pacific-like basin with the short western boundary, the deep sinking appears to be supplied both from the subtropical passive basin and the Southern Ocean (Fig. 13d). For this equilibrium, the same features show a more pronounced basin asymmetry as for the 3525, 3510, and 5010 equilibriums. The northward (southward) heat transport is increased in the active (passive) basin (see Fig. 14) and the surface salinity is decreased in the northern passive basin.

When the deep-water formation occurs in the Atlantic-like basin with the long western boundary, on the other hand, the deep sinking appears to be supplied mainly by

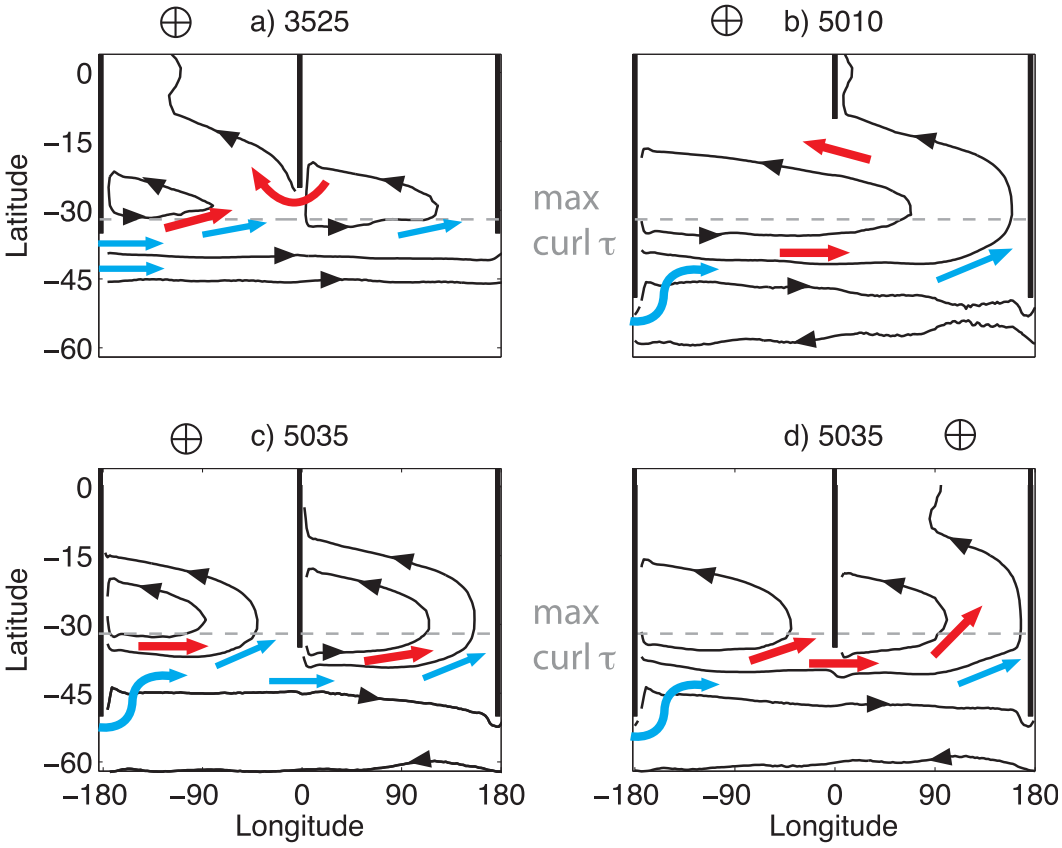

FIG. 13. Schematic of the different regimes of interocean exchange in the simulations with equally wide basins for (a) 3525, (b) 5010, and (d),(e) 5035 experiments. The circles with the cross indicate the basin forming the deep water. The black lines are selected contours of the potential energy anomaly ϕ, which indicates the flow in the thermocline; see Eq. (4). Red arrows depict the circulation of subtropical thermocline water and blue arrows depict the upper-ocean flow of subpolar and Southern Ocean water masses. The gray dashed lines show the position of the Southern Hemisphere maximum of the wind stress curl, essentially collocated with the zero wind line. (a) Atlantic sinking chiefly supplied by the westward warm water path and (c) Atlantic sinking supplied chiefly by eastward the cold water path (e.g., Gordon 1986).

waters derived from the Southern Ocean. Here, the flow into the active basin is reminiscent of the eastward cold water path from the Southern Ocean to the South Atlantic (Gordon 1986; Rintoul 1991). For this equilibrium, the basin asymmetries of the flow are diminished and become weaker than in the 5050 and 3535 equilibriums. Notably, the salinity fields indicate that the inflow to the passive basin is stronger and more saline, resulting in a partial salinification of the passive basin (see Fig. 12).

These results indicate a preference for Pacific sinking in the 5035 geometry, but that the asymmetry in basin geometry is not pronounced enough to remove the Atlantic sinking equilibrium. Indeed, in the Pacific sinking state, the overturning circulation carries salt into the active basin at a rate similar to that seen in the 3535 geometry (Fig. 7). In the Atlantic sinking state, on the other hand, this salt transport is reduced significantly and plays presumably a minor role for the salinification of the active basin. Thus when the Agulhas leakage effect is weak or even overridden, as in the 5035 geometry, additional asymmetries are required for uniquely localizing the Northern Hemisphere sinking to the Atlantic basin. We will show below that a narrowing of the Atlantic basin, which increases the net evaporation over the narrow basin, strongly limits the possibility to establish deep northern sinking in the wide Pacific basin.

3) THE TERMINATION LATITUDES AND THE NATURE OF EQUILIBRIUMS

Figure 14, showing the cross-equatorial heat transport in the active basin, illustrates qualitatively how the nature of asymmetric equilibriums depends on the continental extents when the two basins are equally wide. The lines connecting the simulated heat transports represent our attempt to map out the parameter space. When the

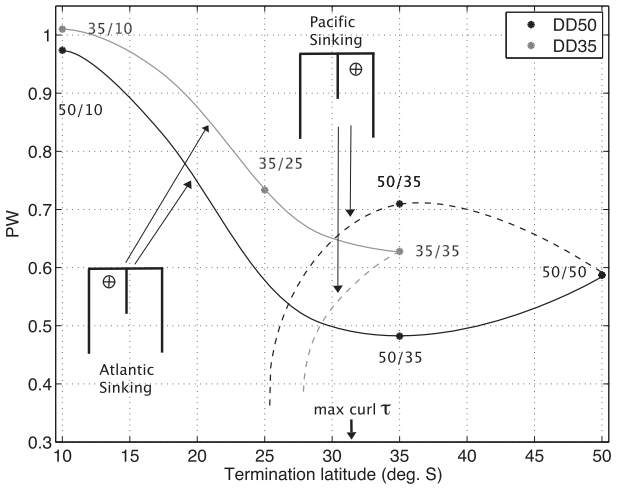

FIG. 14. Qualitative illustration of how the termination latitude of the short continent affects the asymmetric equilibriums in equal-width basins. Here, the basin asymmetry in flow is characterized by the northward heat transport at the equator in the basin forming the deep water. The black asterisks show the 50 experiments, with the long continent at 50°S, and the gray asterisks show the 35 experiments with the long continent at 35°S. The lines show the conjectured dependence of the cross-equatorial heat transport on the termination latitude of the short continent. The solid lines indicate equilibriums with sinking in the Atlantic-like basin with the long western boundary, and the dashed lines indicate equilibriums with sinking in the Pacific-like basin with the short western boundary.

long continent is anchored at 50°S, we note that for the Atlantic sinking state, the active basin overturning and heat transport decrease initially when the eastern African boundary is shortened. The response for the Pacific sinking states is the opposite. As illustrated in Fig. 13, this reflects an enhanced eastward routing of thermocline water. Moreover, when the long continent extends into the subpolar gyre (i.e., beyond about 40°S), there is an enhanced eastward routing of subpolar and Southern Ocean water.

When the African continent passes some latitude near the zero wind line, the interplay between the basin geometry and the subtropical gyres promotes a westward transport of thermocline water into the Atlantic basin. This induces a preference for Atlantic sinking and when Africa is shifted equatorward of a critical latitude, the Pacific sinking state ceases to exist. The ''bowing down'' of the dashed line in Fig. 14 indicates this geometrically induced removal of the Pacific sinking states. Admittedly, the critical latitude of the African continent that uniquely localizes the sinking to the Atlantic basin is poorly constrained by our experiments. However, the 3510 and 5010 experiments suggest that it is the position of the short, rather than the long, continent that is decisive for localizing the sinking to the Atlantic basin.

The notion that the interplay between the wind-driven circulation and the basin geometry sets the preference for which basin that forms the deep water when both basins are equally wide is supported by the ''Switch'' experiments described in appendix B. In these simulations, the model has been initialized with salinity and temperature fields that serve to localize the deep sinking to the basin that does not form deep water in the equilibrated state. In these transient experiments, we find that the oceanic salt transport between the basins is instrumental for the salinification of the basin with the long western boundary. The atmospheric transport of freshwater between the basins serves as a positive feedback, but it is not the initial driver of the salt redistribution when the basins are equally wide.

b. The effect of a difference in basin widths

As emphasized by Ferreira et al. (2010), an asymmetry in the basin width has a strong impact on the atmospheric vapor transport between the basins. The underlying reason is that the evaporation has strong zonal gradients within the basins (see Fig. 4). In the midlatitudes, the strongest evaporation occurs over the poleward flowing currents along the western basin boundaries. In these latitudes, the winds carry the evaporated water vapor eastward. As there is some fetch of the precipitation, the freshwater is brought back to the ocean farther downwind. In a narrow basin, a larger fraction of the evaporation will be carried across the basin boundary and precipitated over the wide basin. This yields a tendency for a salinification of the narrow basin. In reality, the drainage systems over land matter for the strength of this effect.

The impact of a basin-width difference on the freshwater budget can be illustrated by calculating a freshwater transport anomaly[1] ΔF, which is defined through the relations

$$F_A = \lambda F + \Delta F \quad \text{and} \quad F_P = (1-\lambda)F - \Delta F, \qquad (5)$$

where F_A and F_P are the meridional freshwater transport in the active and passive basin, respectively; $F = F_A + F_P$ the total oceanic transport; and λ and $1-\lambda$ the fractional width of the narrow (active) and the wide (passive) basin, respectively. The freshwater transport anomaly ΔF is the departure from the basin-width-weighted fraction of the total oceanic transport and given by

[1] Note that ΔF is identical to the quantity F_S^* used by Ferreira et al. (2010, see their Fig. 8).

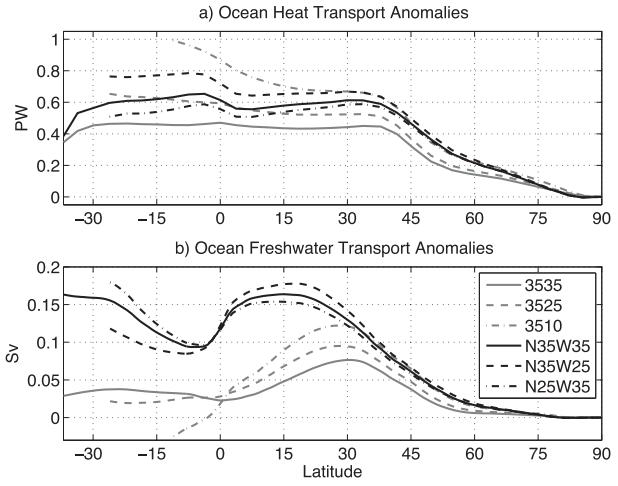

FIG. 15. (a) Ocean heat ΔH and (b) freshwater ΔF transport anomalies, defined by Eqs. (5),(6), for equal-width basin (gray lines) and narrow–wide basin (black lines) experiments. Note that at latitudes where $\partial \Delta F/\partial y < 0$, the zonal-mean $E - P$ is greater per unit area in the active than in the passive basin and vice versa where $\partial \Delta F/\partial y > 0$.

$$\Delta F = (1 - \lambda)F_A - \lambda F_P. \tag{6}$$

If ΔF is positive at a certain latitude, then north of that latitude the net evaporation per unit area is stronger over the active than over the passive basin.

Figure 15 shows the freshwater transport anomalies from the 35-suite experiments including equal-width and narrow–wide basin configurations. Focusing on the two 3535 experiments, we find that near 35°S, ΔF is about 0.03 Sv in the equal-width configuration and 0.16 Sv in the narrow–wide configuration, showing that the basin difference in $E - P$ is strongly amplified by the difference in basin widths. Further details of the freshwater budget in the N35W35 experiment are described by Ferreira et al. (2010).

The sequence from equal to different basin widths in the 3535 experiments results in a reduction of the poleward energy transport in the active basin forming the deep water (see Fig. 11). In the passive basin, the heat transport response is the opposite of that in the active basin. Primarily, this reflects changes in the wind-driven component of the heat transport, which is roughly proportional to the basin width (e.g., Klinger and Marotzke 2000; Nilsson and Körnich 2008). To compensate for the basin-width-related changes in wind-driven circulation, we introduce an ocean heat transport anomaly ΔH, which is defined in the same manner as the freshwater transport anomaly [i.e., $\Delta H = (1 - \lambda)H_A - \lambda H_P$; see Eqs. (5) and (6)]. If the change in heat transport between the equal-width and narrow–wide 3535 experiments would be proportional to the change in basin width, then ΔH would be identical in the two experiments. However, Fig. 15 shows that ΔH is greater in the narrow–wide basin experiment, reflecting that the basin-width difference reinforces the asymmetry in ocean heat transport.

c. *The effects of differences in both basin widths and continent lengths*

In basin configurations where both the continental extents and the basin widths differ, two chief mechanisms control the localization of the deep sinking: the interbasin oceanic salt transport and the atmospheric freshwater transport between the basins. We will here describe experiments designed to examine the relative importance of these two mechanisms for the localization of the sinking. It is relevant to note that the geometries where the basins are equally wide (e.g., 3525) or the continents end at the same latitude (e.g., N35W35) share a symmetry property: the geometry is (dynamically) invariant when the two land barriers are interchanged. The reason is the rotational symmetry of the governing equations, which makes the choice of the zero longitude irrelevant.

In the N35W25 and N25W35 geometries, this symmetry is broken and the interchange of the two land barriers yields to two geometries with different dynamical properties (Fig. 16). From our study of the separate roles of asymmetries in continental lengths and basin widths, we anticipate that the two basin asymmetries in the N35W25 experiment jointly act to localize the deep-water formation to the narrow basin. In the N25W35 experiment, on the other hand, we anticipate that the asymmetry in continental extents will induce a preference for sinking in the wide basin that here has the long western boundary. As it turns out, the asymmetries in basin widths are more important than those in continent lengths in these experiments. In both geometries, the sinking is uniquely localized to the narrow basin.

We have also conducted Switch experiments initialized to yield deep sinking in the wide basin in these two geometries (see appendix B). In both cases, sinking is restored to the narrow basin. The N25W35 Switch (taking longer to adjust because of the competing geometrical effects) demonstrates that the salinification process resulting from basin widths is more effective than that resulting from continental extends. However, if the difference in basin widths would gradually be decreased, a threshold would be reached at which the deep-water formation would relocalize to the slightly wider basin with the long western boundary.

The heat and freshwater transport anomalies, shown in Fig. 15, provide some information on the strength and

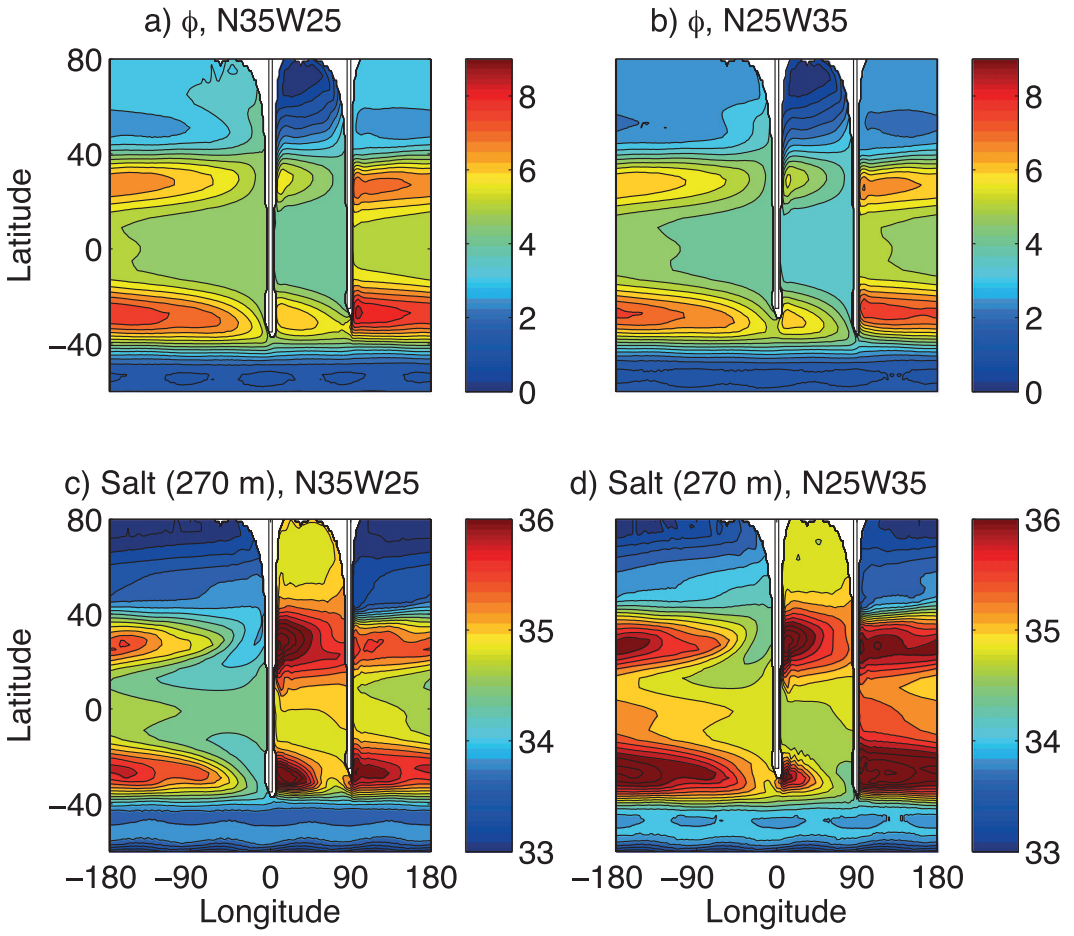

FIG. 16. As in Fig. 8, but for the (a),(c) N35W25 and (b),(d) N25W35 experiments. Note that the deep-water formation remains locked to the narrow basin in the N25W35 experiment, despite that the Agulhas flow acts to export salt from the narrow basin; the wide basin is notably more saline when it receives, rather than supplies, the westward Agulhas flow of thermocline water.

effect of basin asymmetries in continental lengths and basin widths. The 3535 experiment, in which the basins are identical, illustrates the anomaly strengths created only by internal atmosphere–ocean dynamics. We note that the asymmetries in continental lengths have a qualitative similar effect in equal-width and narrow–wide basin experiments. Near the equator the heat transport anomaly ΔH is increased by about 0.1 PW in the sequence from the 3535 to 3525 experiments both in the equal-width and narrow–wide basin configurations. We also note that north of the equator a sequence of geometry change that entails a positive change in ΔH is accompanied by a positive change in ΔF; south of the equator the opposite is true.

Figure 17 shows the Atlantic and Indo-Pacific heat and freshwater transports based on estimates from Trenberth and Caron (2001) and Wijffels et al. (1992). The transports in the narrow and wide basins of the N35W25 experiment are shown for comparison. In addition, we have calculated the heat and freshwater transport anomalies for both the observational estimates and the simulation. The ocean heat transports in the observations and the N35W25 experiment agree remarkably well in the tropics. Poleward of 40°N, the model transports exceed the observed ones. Also, the heat transport anomalies ΔH agree qualitatively, showing that the aqua-planet model yields a leading-order description of the basin partitioning of the ocean heat transport when the asymmetries in basin widths and continental extents are included.

The freshwater transports in the Atlantic and the narrow basin agree qualitatively, but those in the Indo-Pacific and the wide basin deviate significantly poleward of 20°N. This suggests that the partitioning of the freshwater transport between the basins is more sensitive to the details of the land–ocean distribution than

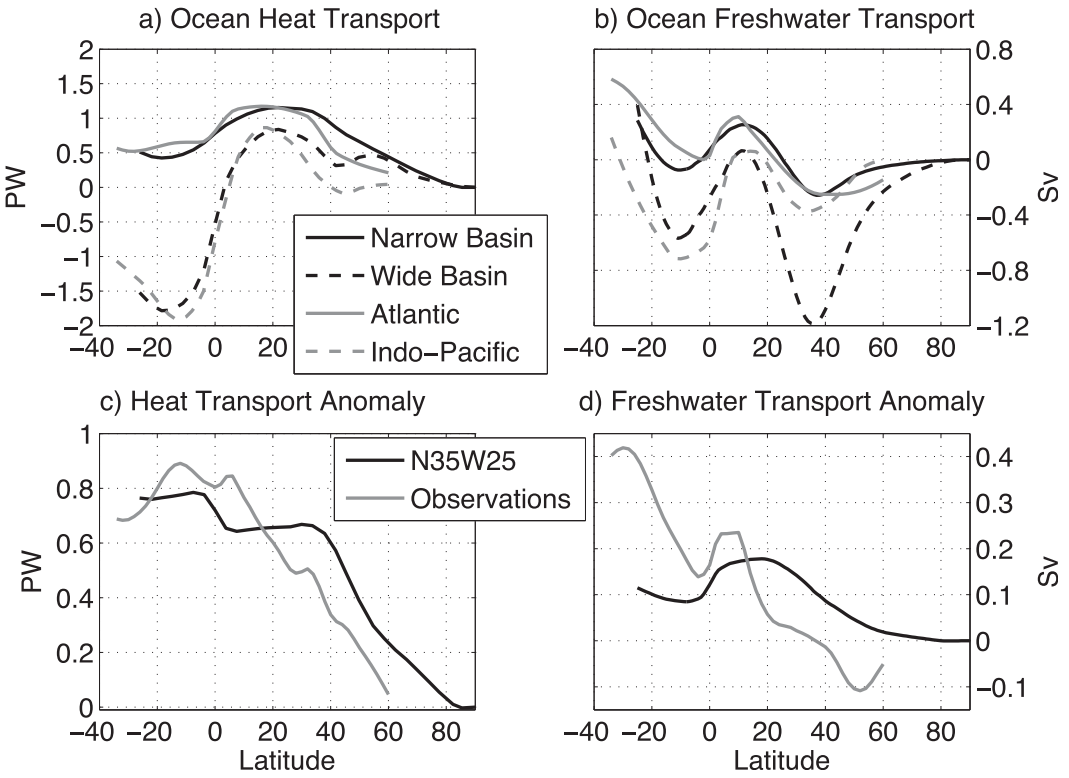

FIG. 17. (a) Ocean heat and (b) freshwater transport in the N35W25 experiment and observations based on estimates from Trenberth and Caron (2001) and Wijffels et al. (1992). Note that the freshwater transport associated with the Bering Strait flow has been removed from the observations. (c),(d) The transport anomalies ΔH and ΔF, defined by Eqs. (5),(6), give the excess transport relative to the total transport multiplied with the fractional basin width λ of the basin forming the deep water. For the observation-based ΔH and ΔF, λ has been calculated using average widths of the Indo-Pacific and Atlantic in bins of 10° latitude, excluding marginal seas such as the Mediterranean.

the partitioning of the heat transport. It can be noted that the observationally based ΔF indicates a stronger basin difference in the net evaporation in the Southern Hemisphere. This anomalous evaporation over the real South Atlantic is presumably important for making the tropical surface salinity greater in the Atlantic than in the aqua-planet simulations (see Fig. 10).

5. Discussion and conclusions

Using a coupled atmosphere–sea ice–ocean model in an aqua-planet setting, we have examined the role of the basin geometry for the climate and ocean circulation. We have focused on a present-day-like setting with two northern basins and a circumpolar ocean in the south and conducted a suite of experiments in which the southward extents of the land barriers and the basin widths have been varied. The main focus has been on the role of these two key asymmetries of the basin geometry for the salinification of the Atlantic Ocean.

In the configurations in which the two basins are identical, we have found symmetric states with deep-water formation in both basins as well as asymmetric states with the deep-water formation localized to one of the basins. The asymmetric states are created by internal atmosphere–ocean dynamics, which spontaneously break symmetry between the basins. It is notable that even these asymmetric states have the main hydrographic features of the real ocean (Fig. 5). Thus, geographical asymmetries are not necessary for obtaining a salinification of the basin that forms the deep water; the oceanic salt–advection feedback is sufficient as has been emphasized by, for instance, Walin (1985) and Marotzke and Willebrand (1991). Furthermore, atmosphere–ocean coupling acts to amplify the basin asymmetry in salinity through a higher net evaporation over the warmer salty basin (Warren 1983).

Asymmetries in the basin geometry can enhance as well as reduce the basin difference in flow that characterizes the asymmetric state in a fully symmetric two-basin geometry. Generally, these changes are comparatively small to the qualitative difference between the asymmetric and symmetric states in the identical

two-basin geometry. However, the basin geometry exerts a critical influence on the coupled atmosphere–ocean dynamics that controls the partitioning of the meridional heat and freshwater transport between the two basins.

The key climate role of the basin-geometry asymmetries is their capacity to uniquely localize the deep-water formation to one of the basins. Our simulations with two equally wide basins show that when the short African continent is located near or equatorward of the zero wind line in the Southern Hemisphere, the deep-water formation becomes uniquely localized to the Atlantic-like basin with the long western boundary (Fig. 14). The mechanistic link is that the maximum curl of the surface wind stress is encountered near the zero wind line; a quantity which in interplay with the basin geometry controls the zonal flow of thermocline water (Sverdrup 1947; de Ruijter et al. 1999; Beal et al. 2011). A westward Sverdrup flow south of the short African continent yields a preference for Atlantic sinking, whereas an eastward Sverdrup flow yields a preference for Pacific sinking (Fig. 13). The time-dependent Switch experiments, described in appendix B, support the notion that the wind-steered interbasin salt transport controls the salinification when the basins are equally wide.

In contrast, when the continents extend equally far south, but the widths of the basins differ, the salinification of the narrow basin seems to be primarily driven by the zonal transport of water vapor in the atmosphere. In this geometry, the narrow basin has a higher net evaporation per unit area than the wide basin (Fig. 15). As demonstrated by Ferreira et al. (2010), this basin difference in $E - P$ is sufficient for uniquely localizing the deep-water formation to the narrow Atlantic-like basin.

In the present experiments, the absence of mountain ranges and detailed land–ocean distribution makes it straightforward to identify the aspects of the basin geometry that control the localization of sinking. Focusing on the N35W25 experiment, it is evident that the sinking is localized to the Atlantic-like basin because it is narrow and the African-like short continent terminates at 25°S, equatorward of the zero wind line. Furthermore, the N25W35 experiment, in which the deep sinking also occurs in the narrow basin, shows that the asymmetry in basin width is more decisive for the localization of the sinking than the difference in continental extents in this particular configuration. Thus, in the present model the detailed features of the land–ocean distribution such as the Atlantic–Arctic connection, the Mediterranean Sea, and the Bering Strait are not necessary for creating a unique equilibrium state with Atlantic sinking, nor is the presence of mountain ranges.

We note that Schmittner et al. (2011) have conducted climate model experiments with present-day basin geometry but where the orography has been scaled down as well as up.[2] In their experiment with completely flat continents, the North Atlantic ceases to form deep water, which is balanced by enhanced Southern Ocean deep sinking and intermediate sinking in the North Pacific. In this flat continent experiment, the whole surface wind field contracts strongly equatorward and the Southern Hemisphere zero wind line is encountered north of the tip of South Africa. As a result, the Agulhas transport into the Atlantic is choked. Thus, the numerical experiments of Schmittner et al. (2011) are broadly consistent with the present results on how the basin geometry influences the localization of the northern sinking. Here, it is relevant to note that meridional shifts of the surface winds have been invoked to explain glacial-to-interglacial changes of the deep-water formation sites in the World Ocean (see, e.g., Bard and Rickaby 2009; Beal et al. 2011, and references therein).

Finally, we underline that the present aqua-planet model has not yielded equilibriums with deep-water formation in the Southern Ocean, which lacks bottom topography and an ''Antarctic'' landmass. Thus, some of the present results may be modified when the boundary conditions allow for deep-water formation in both hemispheres. We believe, however, that the results of how the basin geometry affects the localization of the Northern Hemisphere sinking should remain qualitatively correct as long as equilibrium states exist with sinking in the Northern Hemisphere.

Acknowledgments. The work reported here has been supported by the Swedish Research Council and the NSF Physical Oceanography program as well as by the International Meteorological Institute and the Bert Bolin Centre for Climate Research at Stockholm University. A critical proportion of the work was done during a sabbatical of JN at Scripps Institution of Oceanography; Bill Young, Paula Cessi, and Walter Munk are thanked for their kind assistance and many interesting discussions. We also thank Göran Broström for discussions on the role of dissimilar continental extents for the localization of deep-water formation. J. R. Toggweiler and two anonymous reviewers are thanked for providing insightful comments and suggestions. The simulations have been carried out on the computer Ekman at the PDC Center for High Performance Computing in Stockholm.

[2] Sinha et al. (2012) have conducted similar experiments that yield similar results.

APPENDIX A

Oceanic Freshwater and Salinity Budgets

Consider the volume and salt budget north of a specific latitude y in a basin that is closed in the northern end. Applying the Boussinesq approximation, conservation of volume and salt in the domain V can be written

$$\frac{d}{dt}\int\int\int_V dV = \int\int_{A_{xz}} v\,dA - \int\int_{A_{xy}} (E-P)\,dA \quad \text{and} \tag{A1}$$

$$\frac{d}{dt}\int\int\int_V S\,dV = \int\int_{A_{xz}} vS\,dA + K, \tag{A2}$$

where A_{xz} and A_{xy} are the open boundaries of V, v the meridional velocity, $E - P$ the upward freshwater flux at the sea surface, and K the diffusive salt transport across the southern boundary A_{xz}. Introduce the salinity anomaly

$$\hat{S} \equiv S - S_0, \tag{A3}$$

where S_0 is a constant mean salinity. The fact that $S_0 \gg \hat{S}$ implies that

$$\frac{d}{dt}\int\int\int_V \hat{S}\,dV \approx \int\int\int_V \frac{d\hat{S}}{dt}dV = \int\int\int_V \frac{dS}{dt}dV. \tag{A4}$$

By using this, the volume and salt budgets can be manipulated to yield

$$\int\int\int_V \frac{dS}{dt}dV = S_0\int\int_{A_{xy}} (E-P)\,dA + \int\int_{A_{xz}} v\hat{S}\,dA + K, \tag{A5}$$

where the free surface variations can be neglected when evaluating the term on the left hand side. In a steady state, volume conservation [Eq. (A1)] reduces to

$$0 = F_O - \int\int_{A_{xy}} (E-P)\,dA, \tag{A6}$$

where we have introduced the meridional oceanic freshwater transport

$$F_O \equiv \int\int_{A_{xz}} v\,dA. \tag{A7}$$

The steady-state salt budget can now be written as

$$S_0 F_O + \int\int_{A_{xz}} v\hat{S}\,dA + K = 0. \tag{A8}$$

When discussing steady-state situations, it can be illuminating to refer to the last two terms as the salt transport, despite that the net salt transport is zero.

APPENDIX B

Switch Experiments

For the 3525, 3510, and 5010 geometries, which have equally wide basins, we have only obtained equilibrium states with the sinking in the Atlantic-like basin with the long continent as western boundary. Also for the N35W35, N35W25, and N25W35 geometries, we have only found one type of equilibrium state: the deep-water formation occurs invariably in the narrow basin. We have performed a number of experiments in these geometries, where the model has been initialized with salinity and temperature distributions that serve to establish the deep sinking in the basin that does not form deep water in the equilibrated simulations. We will here discuss one such Switch simulation in detail and briefly mention some results from other experiments.

We have conducted one experiment, labeled N35W25 Switch, which was started with higher salinity in the wide basin and lower salinity in the narrow basin. Figure B1 shows the evolution of the mean basin salinities and the overturning streamfunction in this experiment. Initially, there is deep-water formation and a strong meridional overturning circulation in the wide basin. However, the overturning and the mean basin salinity decrease gradually in the wide basin, whereas the overturning and mean basin salinity increase in the narrow basin. The salinity and flow fields have roughly equilibrated after about 1000 yr, but weaker adjustments continue even after 2000 yr. The evolution is similar to that seen in the N35W35 Switch experiment conducted by Ferreira et al. (2010, see their Figs. A1 and A2).

To examine the relative importance of atmospheric and oceanic interbasin transports of freshwater for the redistribution of salt in the N35W25 Switch experiment, we consider the salinity budget for the narrow and wide basins and the ocean south of 25°S. The basin budgets can be formulated as [see Eq. (A5)]

$$\frac{dS_{NB}}{dt} = \Phi_{NB} + F_{NB}, \tag{B1}$$

$$\frac{dS_{WB}}{dt} = \Phi_{WB} + F_{WB}, \quad \text{and} \tag{B2}$$

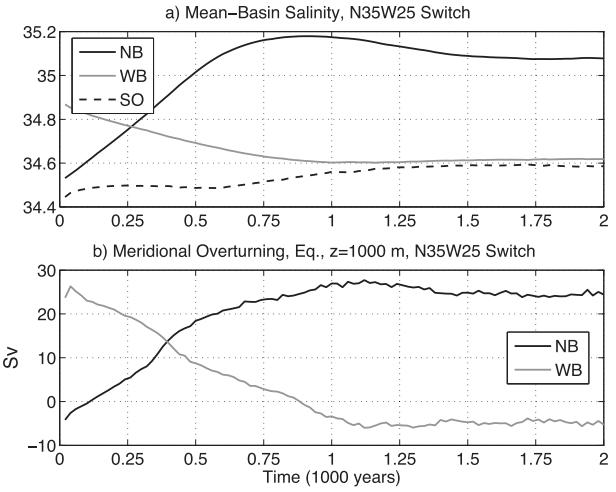

FIG. B1. Time series of (a) basin-mean salinities and (b) meridional overturning at 1000 m on the equator in the N35W25 Switch simulation. The simulation was started with high salinity in the wide basin, where initially the deep-water formation occurred. In (a) the basin-mean salinities are shown for the narrow (NB) and wide (WB) basins as well as for the ocean south of 25°S (SO).

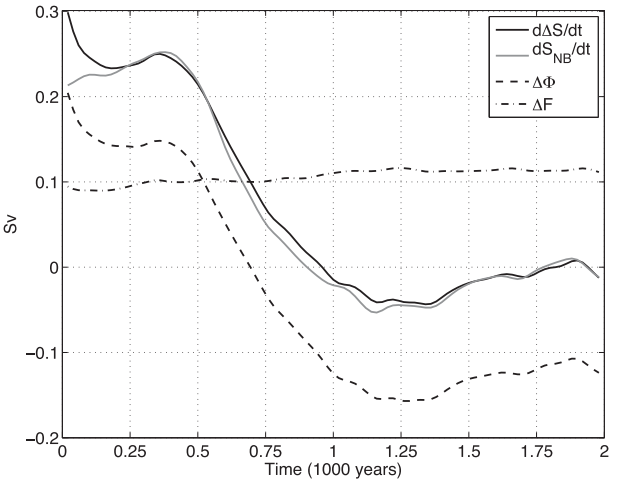

FIG. B2. The evolution of the basin salinity budget (north of 25°S) in the N35W25 Switch simulation. The solid black and gray lines show the rate of change of the basin difference anomaly ΔS [see Eq. (B5) for details] and the mean salinity in the narrow basin. The dashed and the dashed–dotted lines show the contribution to the rate of change in ΔS because of oceanic advection and atmospheric freshwater transports, respectively.

$$\frac{dS_{\mathrm{SO}}}{dt} = -\Phi_A - \Phi_P + F_S. \tag{B3}$$

Here, the subscripts NB and WB denote the narrow and wide basins, respectively, and SO refers to the ocean south of 25°S. The term Φ represents the advective and diffusive salt transport (divided by S_0) and we also have introduced

$$S_{\mathrm{NB}} \equiv \frac{1}{S_0}\int\int\int_{V_{\mathrm{NB}}} S\,dV, \quad F_{\mathrm{NB}} \equiv \int\int_{A_{\mathrm{NB}}} (E-P)\,dA, \tag{B4}$$

where S_0 is the mean salinity and S the salinity, and F_{NB} is the net flux of freshwater to the atmosphere; the definitions are analogous for the quantities pertaining to the other two basins. Note that the storage of freshwater in the atmosphere is small, implying that $F_{\mathrm{NB}} + F_{\mathrm{WB}} + F_{\mathrm{SO}} = 0$. We focus on the basin-width weighted difference in salinity, advection, and atmospheric transports, which are defined by

$$\Delta S = (1-\lambda)S_{\mathrm{NB}} - \lambda S_{\mathrm{WB}}, \tag{B5}$$

$$\Delta\Phi = (1-\lambda)\Phi_{\mathrm{NB}} - \lambda\Phi_{\mathrm{WB}}, \quad \text{and} \tag{B6}$$

$$\Delta F = (1-\lambda)F_{\mathrm{NB}} - \lambda F_{\mathrm{WB}}, \tag{B7}$$

where λ is the fractional with of the narrow basin (¼ in this case). From the Eqs. (B1) and (B2), it follows that

$$\frac{d\Delta S}{dt} = \Delta\Phi + \Delta F. \tag{B8}$$

Figure B2 shows the ΔS budget for the N35W25 Switch experiment. From the very start, the narrow basin exports freshwater via the atmosphere to the wide basin. However, initially the rate of change in ΔS is dominated by the salt advection between the basins. After about 700 yr, the salt advection changes sign, implying an advective export of salt transport out of the narrow basin. Near year 2000, this salt export (or freshwater import) balances the basin-width weighted freshwater export via the atmosphere ΔF.

Both oceanic salt advection and atmospheric freshwater transport contribute to the flow transition in the N35W25 Switch experiment. In the N35W35 Switch experiment of Ferreira et al. (2010), the atmospheric freshwater transport appears to dominate the transition. In the 3510 and 5010 Switch experiments (not shown), however, the basin with the short western boundary is warmer initially and exports freshwater to the basin with the long western boundary. At the start of the 3510 Switch experiment, ΔF is about -0.05 Sv, implying that the basin $E - P$ difference acts to sustain the deep-water formation in the Pacific-like basin. However, the advective salt transport $\Delta\Phi$, which is directed into the Atlantic-like basin, is initially about 0.25 Sv. Accordingly, the salinification of the Atlantic-like basin is driven by ocean salt advection, rather than by atmospheric freshwater transport between the basins in the 3510 Switch experiment.

The evolution of the basin salinity difference has a comparable time scale in the 3510, 5010, and N35W25 Switch experiments. In the 3525 and N25W35 Switch experiments, the transitions are significantly slower, taking 4000–5000 yr to be completed (not shown). The much longer adjustment time scales encountered in these two geometries reflect that the basin asymmetries yield a weaker localization of the deep-water formation than in the 3510 and N35W25 geometries.

REFERENCES

Adcroft, A., J. M. Campin, C. Hill, and J. Marshall, 2004: Implementation of an atmosphere–ocean general circulation model on the expanded spherical cube. *Mon. Wea. Rev.,* **132,** 2845–2863.

Bard, E., and R. E. M. Rickaby, 2009: Migration of the subtropical front as a modulator of glacial climate. *Nature,* **460,** 380–383.

Barron, E. J., W. H. Peterson, D. Pollard, and S. Thompson, 1993: Past climate and the role of ocean heat transport: Model simulations for the Cretaceous. *Paleoceanography,* **8,** 785–798.

Beal, L. M., and Coauthors, 2011: On the role of the Agulhas system in ocean circulation and climate. *Nature,* **472,** 429–436.

Broecker, W. S., D. M. Peteet, and D. Rind, 1985: Does the ocean–atmosphere system have more than one stable mode of operation? *Nature,* **315,** 21–26.

Bryden, H. L., B. A. King, and G. D. McCarthy, 2011: South Atlantic overturning circulation at 24°S. *J. Mar. Res.,* **69,** 39–56.

Campin, J. M., J. Marshall, and D. Ferreira, 2008: Sea ice–ocean coupling using a rescaled vertical coordinate *z*. *Ocean Modell.,* **24,** 1–14.

Corell, H., J. Nilsson, K. Döös, and G. Broström, 2009: Wind sensitivity of the inter-ocean heat exchange. *Tellus,* **61A,** 635–653.

Czaja, A., 2009: Atmospheric control on the thermohaline circulation. *J. Phys. Oceanogr.,* **39,** 234–247.

De Boer, A. M., J. R. Toggweiler, and D. M. Sigman, 2008: Atlantic dominance of the meridional overturning circulation. *J. Phys. Oceanogr.,* **38,** 435–450.

de Ruijter, W. P. M., A. Biastoch, S. Drijfhout, J. Lutjeharms, R. Matano, T. Pichevin, P. J. van Leeuwen, and W. Weijer, 1999: Indian-Atlantic interocean exchange: Dynamics, estimation and impacts. *J. Geophys. Res.,* **104** (C9), 20 885–20 910.

Dijkstra, H. A., and W. Weijer, 2005: Stability of the global ocean circulation: Basic bifurcation diagrams. *J. Phys. Oceanogr.,* **35,** 933–948.

Enderton, D., and J. C. Marshall, 2009: Explorations of atmosphere–ocean–ice climates on an aquaplanet and their meridional energy transports. *J. Atmos. Sci.,* **66,** 1593–1611.

Ferreira, D., J. Marshall, and J.-M. Campin, 2010: Localization of deep-water formation: Role of atmospheric moisture transport and geometrical constraints on ocean circulation. *J. Climate,* **23,** 1456–1476.

Gent, P. R., and J. C. McWilliams, 1990: Isopycnal mixing in ocean circulation models. *J. Phys. Oceanogr.,* **20,** 150–155.

Gill, A. E., 1973: Circulation and bottom water production in the Weddell Sea. *Deep-Sea Res.,* **20,** 111–140.

Gordon, A. L., 1986: Interocean exchange of thermocline water. *J. Geophys. Res.,* **91** (C4), 5037–5046.

Hawkins, E., R. S. Smith, L. C. Allison, J. M. Gregory, T. J. Woollings, H. Pohlmann, and B. de Cuevas, 2011: Bistability of the Atlantic overturning circulation in a global climate model and links to ocean freshwater transport. *Geophys. Res. Lett.,* **38,** L10605, doi:10.1029/2011GL047208.

Hughes, T. C. M., and A. J. Weaver, 1994: Multiple equilibria of an asymmetric two-basin ocean model. *J. Phys. Oceanogr.,* **24,** 619–637.

Huisman, S., 2010: On multiple equilibria of the global ocean circulation and the preference for North Atlantic sinking. Ph.D. thesis, Utrecht University, 118 pp.

——, H. A. Dijkstra, A. S. von der Heydt, and W. P. M. de Ruijter, 2009: Robustness of multiple equilibria in the global ocean circulation. *Geophys. Res. Lett.,* **36,** L01610, doi:10.1029/2008GL036322.

Johnson, H. L., D. P. Marshall, and D. A. J. Sproson, 2007: Reconciling theories of a mechanically driven meridional overturning circulation and multiple equilibria. *Climate Dyn.,* **29,** 821–836.

Klinger, B. A., and J. Marotzke, 2000: Meridional heat transport by the subtropical cell. *J. Phys. Oceanogr.,* **30,** 696–705.

——, J. Marshall, and U. Send, 1996: Representation of convective plumes by vertical adjustment. *J. Geophys. Res.,* **101** (C8), 18 175–18 182.

Manabe, S., and R. J. Stouffer, 1999: The role of thermohaline circulation in climate. *Tellus,* **51A,** 91–109.

Marotzke, J., and J. Willebrand, 1991: Multiple equilibria of the global thermohaline circulation. *J. Phys. Oceanogr.,* **21,** 1372–1385.

Marshall, J., and K. Speer, 2012: Closure of the meridional overturning circulation through Southern Ocean upwelling. *Nat. Geosci.,* **5,** 171–180.

——, A. Adcroft, C. Hill, L. Perleman, and C. Heisey, 1997a: A finite-volume, incompressible Navier Stokes model for studies of the ocean on parallel computers. *J. Geophys. Res.,* **102** (C3), 5753–5766.

——, C. Hill, L. Perleman, and A. Adcroft, 1997b: Hydrostatic, quasi-hydrostatic, and non-hydrostatic ocean modeling. *J. Geophys. Res.,* **102** (C3), 5733–5752.

——, A. Adcroft, J. M. Campin, C. Hill, and A. White, 2004: Atmosphere–ocean modeling exploiting fluid isomorphisms. *Mon. Wea. Rev.,* **132,** 2882–2894.

McCreary, J. P., and P. Lu, 1994: Interaction between the subtropical and equatorial ocean circulations: The subtropical cell. *J. Phys. Oceanogr.,* **24,** 466–497.

Mikolajewicz, U., E. Maier-Reimer, T. Crowley, and K. Kim, 1993: Effects of Drake and Panamanian gateways on the circulation of an ocean model. *Paleoceanography,* **8,** 409–426.

Molteni, F., 2003: Atmospheric simulations using a GCM with simplified physical parametrizations. I: Model climatology and variability in multidecadal experiments. *Climate Dyn.,* **20,** 175–191.

Nilsson, J., and H. Körnich, 2008: A conceptual model of the surface salinity distribution in the oceanic Hadley cell. *J. Climate,* **21,** 6586–6598.

Pedlosky, J., 1996: *Ocean Circulation Theory.* Springer-Verlag, 453 pp.

Rahmstorf, S., 1996: On the freshwater forcing and transport of the Atlantic thermohaline circulation. *Climate Dyn.,* **12,** 799–811.

Redi, M. H., 1982: Oceanic isopycnal mixing by coordinate rotation. *J. Phys. Oceanogr.,* **12,** 1154–1158.

Reid, J. L., 1961: On the temperature, salinity, and density differences between the Atlantic and Pacific Oceans in the upper kilometre. *Deep-Sea Res.,* **7,** 265–275.

——, 1979: On the contribution of the Mediterranean Sea outflow to the Norwegian-Greenland Sea. *Deep-Sea Res.,* **26A,** 1199–1223.

Rintoul, S. S., 1991: South Atlantic interbasin exchange. *J. Geophys. Res.,* **96** (C2), 2675–2692.

Schmittner, A., T. A. M. Silva, K. Fraedrich, E. Kirk, and F. Lunkeit, 2011: Effects of mountains and ice sheets on global ocean circulation. *J. Climate,* **24,** 2814–2829.

Seager, R., D. S. Battisti, J. Yin, N. Naik, N. Gordon, A. C. Clement, and M. A. Cane, 2002: Is the Gulf Stream responsible for Europe's mild winters? *Quart. J. Roy. Meteor. Soc.,* **128,** 2563–2586.

Sijp, W. P., and M. H. England, 2008: Effect of a northward shift in the Southern Hemisphere westerlies on the global ocean. *Prog. Oceanogr.,* **79,** 1–9.

——, and ——, 2009: Southern Hemisphere westerly wind control over the ocean's thermohaline circulation. *J. Climate,* **22,** 1277–1286.

Sinha, B., A. T. Blaker, J. J.-M. Hirschi, S. Bonham, M. Brand, S. Josey, R. S. Smith, and J. Marotzke, 2012: Mountain ranges favour vigorous Atlantic meridional overturning. *Geophys. Res. Lett.,* **39,** L02705, doi:10.1029/2011GL050485.

Smith, R. S., C. Dubois, and J. Marotzke, 2006: Global climate and ocean circulation on an aquaplanet ocean–atmosphere general circulation model. *J. Climate,* **19,** 4719–4737.

Stommel, H. M., 1961: Thermohaline convection with two stable regimes of flow. *Tellus,* **13,** 224–230.

——, and G. T. Csanady, 1980: A relation between the T-S curve and global heat and atmospheric water transport. *J. Geophys. Res.,* **85** (C1), 495–501.

Sverdrup, H. U., 1947: Wind-driven currents in a baroclinic ocean: With application to the equatorial currents of the eastern Pacific. *Proc. Natl. Acad. Sci. USA,* **33,** 318–326.

Toggweiler, J. R., and B. Samuels, 1995a: Effect of Drake Passage on the global thermohaline circulation. *Deep-Sea Res.,* **42,** 477–500.

——, and ——, 1995b: Effect of sea ice on the salinity of Antarctic bottom waters. *J. Phys. Oceanogr.,* **25,** 1980–1997.

Trenberth, K. E., and J. M. Caron, 2001: Estimates of meridional atmosphere and ocean heat transports. *J. Climate,* **14,** 327–347.

Walin, G., 1985: The thermohaline circulation and the control of ice ages. *Palaeogeogr. Palaeoclimatol. Palaeoecol.,* **50,** 323–332.

Warren, B. A., 1983: Why is no deep water formed in the North Pacific? *J. Mar. Res.,* **41,** 327–347.

Weaver, A. J., C. M. Bitz, A. F. Fanning, and M. M. Holland, 1999: Thermohaline circulation: High-latitude phenomena and the difference between the Pacific and Atlantic. *Annu. Rev. Earth Planet. Sci.,* **27,** 231–285.

Weyl, P. K., 1968: The role of the oceans in climate change: A theory of the ice ages. *Causes of Climatic Change, Meteor. Monogr.,* No. 30, Amer. Meteor. Soc., 37–62.

Wijffels, S. E., R. W. Schmitt, H. L. Bryden, and A. Stigebrandt, 1992: Transport of freshwater by the ocean. *J. Phys. Oceanogr.,* **22,** 155–162.

Winton, M., 2000: A reformulated three-layer sea ice model. *J. Atmos. Oceanic Technol.,* **17,** 525–531.

Wolfe, C. L., and P. Cessi, 2011: The adiabatic pole-to-pole overturning circulation. *J. Phys. Oceanogr.,* **41,** 1795–1810.